Energy & Environmental Science

PERSPECTIVE

Cite this: *Energy Environ. Sci.*, 2014, **7**, 3952

A perspective on the production of dye-sensitized solar modules

Azhar Fakharuddin,[a] Rajan Jose,*[a] Thomas M. Brown,[b] Francisco Fabregat-Santiago[c] and Juan Bisquert*[cd]

Dye-sensitized solar cells (DSCs) are well researched globally due to their potential as low-cost photovoltaic (PV) devices especially suited for building and automobile integrated PV (BIPV, AIPV) and portable or indoor light harvesting applications. Since 1991, large monetary and intellectual investments have been made to develop DSCs into deployable technologies, creating a wealth of knowledge about nano-interfaces and devices through an increasing number of research reports. In response to these investments, the dawn of the new millennium witnessed the emergence of a corporate sector of DSC development. Advances in their design, their incorporation on flexible substrates, the development of solid state modules, their enhanced stability in outdoor environments, and their scalable fabrication tools and techniques have allowed DSCs to move from the laboratory to real-life applications. Although photoconversion efficiencies are not on a par with commercially available CIGS or single crystalline silicon solar cells, they possess many features that compel the further development of DSC modules, including transparency, light weight, flexibility, conformability, workability under low-light conditions, and easy integration in buildings as solar windows. In fact, DSC panels have been shown to deliver even more electricity than their silicon and thin film counterparts of similar power ratings when exposed to low light operating conditions due to their workability in such conditions; thus, they are potential market leaders in BIPV and indoor light harvesting photovoltaic technology. However, large area dye-solar modules lack in performance compared to their laboratory scale devices and also suffer from long term stability issues. Herein, we discuss the main factors behind their inferior photovoltaic performance and identify possible opportunities for the design of more efficient DSC modules.

Received 4th June 2014
Accepted 8th September 2014

DOI: 10.1039/c4ee01724b

www.rsc.org/ees

Broader context

Dye-sensitized solar cells represent a sustainable cheap solar electricity domain; working under the framework of nanotechnology, these modern devices have opened up new opportunities for economic development. This article aims to cater to the need for a diverse readership from academic researchers for an overview of progress made in developing dye solar science to an adapted technology and subsequent "need driven" studies to solve critical issues to entrepreneurs to identify key opportunities in the dye-solar business, to corporations to obtain an overview of the current state of affairs in dye-solar technology. We address many questions relevant to dye-solar research, development, and business: how far are the state-of-the art dye-sensitized solar modules from exhibiting characteristics of a matured technology to guarantee its promise as a medium for cheap solar electricity? What is the size of the industrial sector, and what are their core businesses? What are the different designs employed in dye-solar modules? What are the areas requiring innovations to further develop dye-solar modules? These studies lead us to conclude that, at the moment, dye-solar modules appear as an undergraduate student who offers enormous possibilities, although many problems are yet to be solved before being considered as mature!

1. Introduction—renewable energy scenario

The development of a primary supply of clean and sustainable energy is a top global issue. A great portion of today's energy demand (>85%) is fulfilled by fossil fuel-based resources at the expense of global warming and the consequent severe changes in climate.[1] The statistics of increasing energy demand and depleting fossil fuels are alarming: (i) the energy demand is expected to increase two-fold by 2050; and (ii) due to depleting fossil fuel reserves, an additional energy demand equal to

[a]*Nanostructured Renewable Energy Materials Laboratory, Faculty of Industrial Sciences & Technology, Universiti Malaysia Pahang, 26300, Malaysia*
[b]*C.H.O.S.E. (Centre for Hybrid and Organic Solar Energy), Department of Electronic Engineering, University of Rome-Tor Vergata, via del Politecnico 1, 00133, Rome, Italy*
[c]*Photovoltaic and Optoelectronic Devices Group, Departament de Física, Universitat Jaume I, 12071 Castelló, Spain*
[d]*Department of Chemistry, Faculty of Science, King Abdulaziz University, Jeddah, Saudi Arabia*

today's total energy consumption is expected in the next three decades.[2,3] Renewable energy resources such as solar and wind are potentially cost effective, abundant in nature, and evenly distributed across the globe; therefore, they have the potential to help alleviate this energy gap.[4] These resources also eliminate the environmental issues associated with the use of fossil fuels. Among renewable energy resources, solar energy alone has the potential to meet the world's primary energy demand, which would require covering less than 0.4% of our planet's surface with 15% efficient solar panels.[5] Alternatively, using 25% efficient solar panels, a solar farm with an area of ~400 km × 400 km in the Sahara desert would meet the projected energy demand. Above all, energy from sunlight is 200 times more abundant than all other renewable energy resources combined.[3]

The photovoltaic effect was discovered in the 19th century by Edmond Becquerel. Subsequently, solar energy appears not only as a promising alternative energy resource, but also as a better off-grid choice in remote applications and portable electronics. Solar cell technology can be divided into three types: (i) crystalline silicon solar cells; (ii) thin film solar cells ($CuInGaSe_2$, CdTe, a-Si:H, *etc.*), which are called thin because their working electrode comprises much thinner films (~1 μm) than that of the first generation (~350 μm); and (iii) molecular absorber solar cells, in which molecules or inorganic clusters are the primary absorbers, including polymer solar cells, dye-sensitized solar cells (DSCs), quantum dot solar cells, and the recently-developed perovskite solar cells. Over half a century of research in silicon-based solar cells, which currently dominate the photovoltaic market, have resulted in an installed capacity of >40 GW, up from 1.5 GW in 2000 (Fig. 1).[6] As a result, solar cells (mostly silicon-based) currently contribute to energy demands in peak hours. In Germany, ~5.3% of daily demand is fulfilled by solar electricity; this value increases to 20% on longer sunny days.[4,7] Commercial modules of silicon-based solar cells (first generation) with efficiencies (η) of up to ~20% are commercially available. On the other hand, thin film solar cells (second generation) based on $CuInGaSe_2$ (CIGS) have achieved η >20% on a laboratory scale,[8,9] and commercial modules with $\eta \sim 15\%$ are commercially available.[10] Despite the rapidly increasing global installations, many of the first and second generation solar cells still suffer from drawbacks such as long payback, relatively high costs associated with the extreme purity requirement for the active material, scarcity of materials such as indium and silver, and low working capability in cloudy conditions or shaded regions.[4,11] Additionally, due to their opacity (for example, silicon solar cells), these solar cells are not an option for integration into buildings. These drawbacks

Azhar Fakharuddin obtained his bachelor's degree in electronic engineering from Mehran University of Engineering & Technology, Pakistan and Master's degree in electronic engineering from Universiti Malaysia Pahang (UMP). He is currently pursuing doctoral research at the Nanostructured Renewable Energy Materials Laboratory of UMP on the scalability issues of dye-sensitized solar cells (DSCs). His work is primarily focused on investigating the charge transport parameters while upscaling DSCs and exploring appropriate device designs and material architectures to improve charge collection efficiency in large area photoelectrodes. His research interests also include the synthesis and characterisation of metal oxide semiconductors for organic photovoltaics, particularly dye and perovskite-sensitized solar cells/modules. Email: clife03@yahoo.com.

Rajan Jose is a Professor of Materials Science and Engineering at the Faculty of Industrial Sciences and Technology, Universiti Malaysia Pahang (UMP). He supervises the Nanostructured Renewable Energy Materials Laboratory in the UMP. He conducted his doctoral research at the Council of Scientific and Industrial Research (CSIR), Trivandrum, India and received a PhD degree in 2002 for his work on nanostructured perovskite ceramics for microwave and superconducting electronics. He has worked at various capacities at the Indira Gandhi Centre for Atomic Research (India), AIST (Japan), Toyota Technological Institute (Japan), and the National University of Singapore (Singapore) before joining UMP. He has published over 100 papers in SCI journals. He holds over 20 patents nationally and internationally. His h-index is 29 and his g-index is currently 50. His research interests include nanostructured materials and renewable energy devices. E-mail: rjose@ump.edu.my/joserajan@gmail.com.

Thomas M. Brown investigated polymer OLEDs for his PhD at the Cavendish Laboratory, University of Cambridge. From 2001–2005 he developed E-paper as a Senior Engineer with Plastic Logic Ltd. In 2005 he was recipient of a "Re-entry" Fellowship awarded by the Italian Ministry of Education, University and Research and is an Associate Professor at the Department of Electronic Engineering, University of Rome-Tor Vergata. Cofounder of the Centre for Hybrid and Organic Solar Energy, his current research is in dye-sensitized, perovskite, and polymer solar cells. He is on the Advisory Board of Dyepower and is the author of over 100 publications including 16 patents. E-mail: thomas.brown@uniroma2.it.

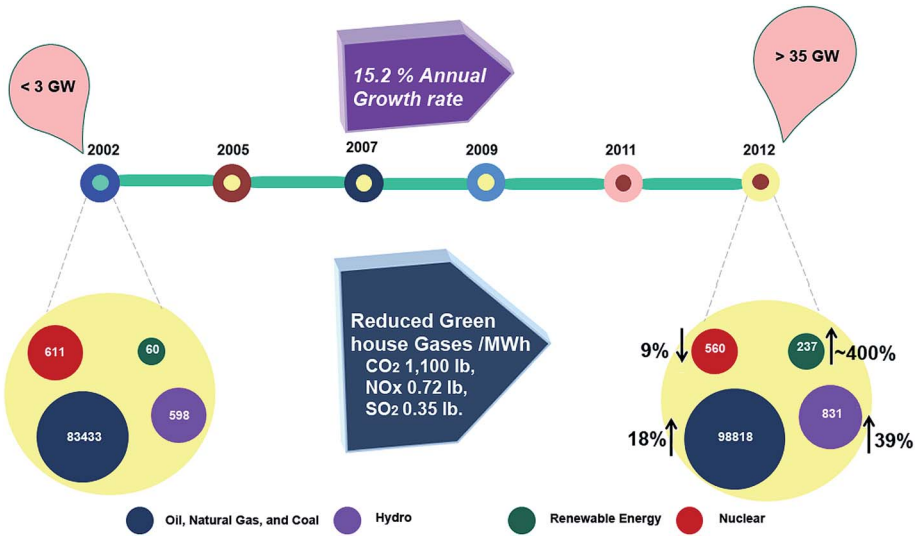

Fig. 1 (a) A chart showing the paradigm shift in the share of renewable energy sources (data collected from ref. 12 and 13). The values are in million tons of oil equivalents (mtoe).

necessitate the third generation photovoltaics, which aim to resolve many of the issues of the first two generations. Although the initial development of these new photovoltaics involved delivering applications and building integrated photovoltaics (BIPV; *e.g.*, automotive integrated photovoltaics, AIPV), further reducing their costs remains an important target as the cost of silicon solar cells has significantly dropped in recent years. However, the third generation devices currently generally suffer from lower η and short term outdoor stability compared to the other two well-established photovoltaic generations.

The purpose of this article is to review the progress made in deploying a third generation solar cell – the dye-sensitized solar cell (DSC) – from the laboratory scale to real life application. A photoconversion efficiency comparable to that of market-leading CIGS or single crystalline silicon solar cells is yet to be achieved by DSCs; however, their positive inherent features such as workability under low-light conditions, transparency, flexibility, conformability, superior performance under low-level or indoor light and easy integration in buildings as solar windows will facilitate their market entry. This article is

Francisco Fabregat-Santiago is an Associate Professor in the Physics Department of Universitat Jaume I de Castelló (Spain). He is an expert in electro-optical characterisation of devices and particularly known by his works on the use of impedance spectroscopy to model, analyse and interpret the electrical characteristics (charge accumulation, transfer reactions and transport) of devices and films including ZnO and TiO_2 nanostructured films (nanocolloids, nanorods and nanotubes), dye-sensitized and quantum dot solar cells, electrochromic materials and liquid and solid state hole conductors. His latest research is focused on perovskite solar cells, photoinduced water splitting, microbial fuel cells and bio-sensors. He has published 85 papers that have accumulated more than 4000 citations with an h-index of 31. Email: fran.fabregat@fca.uji.es.

Juan Bisquert is a professor of applied physics at Universitat Jaume I de Castelló, Spain (http://www.elp.uji.es/jb.php). He conducts experimental and theoretical research on nanoscale devices for the production and storage of clean energies. His main topics of interest are materials and processes in perovskite solar cells, nanostructured solar cells, solar fuel production, and lithium batteries. He has developed the application of measurement techniques and physical modelling of nanostructured energy devices that relate the device operation to the elementary steps taking place at the nanoscale: charge transfer, carrier transport, chemical reaction, etc., *especially in the field of impedance spectroscopy, as well as general device models. He has authored 280 peer reviewed papers, has an h-index of 53, and is currently a Senior Editor of the Journal of Physical Chemistry and a member of Editorial Board of Energy and Environmental Science, and ChemElectroChem. E-mail: bisquert@fca.uji.es.*

organized as follows. Section 2 outlines the working principle, various components and types of laboratory scale DSCs. Section 3 compares the outstanding features of DSC technology that facilitate its entry into the photovoltaic market, and Section 4 discusses their worldwide business growth. Sections 5–9 elaborate on the developments in dye-solar modules (DSMs). Section 10 critically analyses the major factors in the inferior performance of DSMs and introduces alternative designs for these modules. Research on the long term stability of DSMs is reviewed in Section 11, while Section 12 talks about the standards required to advance DSCs from the laboratory to successful commercial application. In Section 13, we conclude our observations and make recommendations for future research on high performance and cost effective DSMs.

2. Dye-sensitized solar cells

Among the various types of 3rd generation solar cells, DSCs are promising as they are cost effective, relatively easy to fabricate on large panels, lightweight and flexible; they also offer transparency compared to the first two generations of solar cells.[14–16] Due to their unique transparency,[17] DSCs can easily be integrated into BIPVs and AIPVs; however, outdoor long term stability is yet to be achieved. DSCs have also shown superior performance under indoor lighting[18] and have been developed extensively on flexible substrates.[19] Many reports have been published on the phenomenology of photovoltaic action in DSCs and on the various materials used.[20–22] The DSC is a photoelectrochemical device in which the photocurrent is generated at a junction between a dye-anchored metal oxide semiconductor and a hole-conducting electrolyte upon light absorption. Various materials and their interfaces constituting the DSCs along with the photochemical process are presented in Fig. 2.

DSCs are promising due to their low cost fabrication compared to the first two generations of solar cells; however, their η is much lower than commercially available thin film and silicon solar modules. Although η values up to ~13% have been reported in DSCs,[26] the certified value is ~11.9% for devices built on rigid substrates (fluorine-doped tin oxide (FTO)-coated glass)[9] and ~7.6% for those built on flexible substrates (polyethylene terephthalate (PET)/indium tin oxide (ITO)).[27] As shown in Fig. 3, independent certifications for other types of DSCs such as solid state DSCs (s-DSCs), p-type DSCs (p-DSCs), and tandem DSCs (T-DSCs) are yet to be seen. In view of commercial applications, the outdoor stability of solar panels is crucial in addition to their η value. For example, amorphous silicon (~10%) and organic thin film modules (6.8%) with η values much lower than the certified value of DSMs (8.2%) are commercially available due to their significantly higher lifetimes (~20 years for thin film modules).[28] Although DSCs have shown significant stabilities in indoor accelerated testing,[29,30] the lifetimes of liquid electrolyte-based DSCs (l-DSCs) are far lower in outdoor conditions due to their high volatility. Alternatively, s-DSCs have been developed in order to overcome some of the issues related to the liquid electrolytes. Future research on s-DSCs will be dedicated to solving their primary issues such as poor pore filling (infiltration of the hole transport material into mesoporous MOS), inferior hole mobility and hole diffusion length in these devices. The T-DSCs are also

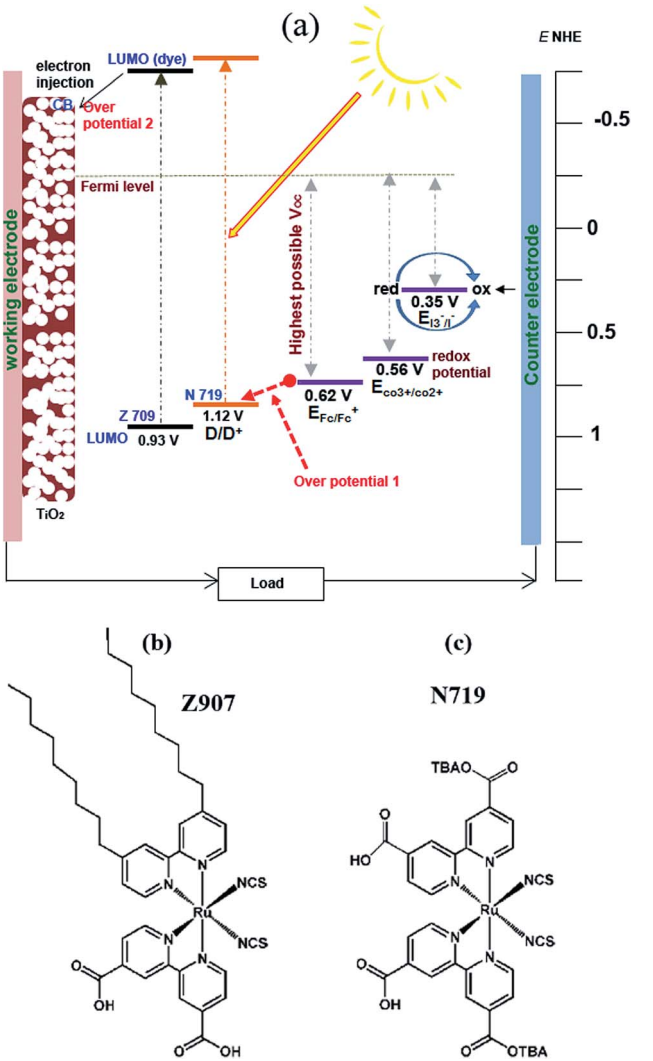

Fig. 2 Schematic of the working mechanism of a DSC. N719 and Z907 are ruthenium-based dyes. $E_{CO^{3+}}$, E_{Fc/Fc^+}, and $E_{I_3^-/I^-}$ are the electrochemical potentials of the cobalt, ferrocene and iodide electrolytes, respectively, measured with respect to a standard hydrogen electrode (NHE). The working electrode (WE) is a mesoporous film of a metal oxide semiconductor (MOS, usually TiO_2) with a thickness of ~3–20 μm coated on a conducting glass substrate. The film is then conjugated with a molecular absorber (dye); a junction is made by putting the film in contact with an electrolyte followed by sealing with a conducting counter electrode (CE) equipped with a catalyst layer. Upon absorption of sunlight, the dye oxidizes and injects the photogenerated electrons into the MOS, which are collected at the WE. The oxidized dye is regenerated by accepting electrons from the redox couple. The electron travels to the CE *via* an external circuit and completes the cycle. Fractions of absorbed energy are lost at the dye–TiO_2 interface (overpotential #1) and the dye–electrolyte interface (overpotential #2). The rest, *i.e.*, {absorbed energy − (overpotential #1 + overpotential #2)}, contribute to the open circuit voltage (V_{OC}). The redox potentials and HOMO level of the dyes are taken from ref. 23 and 24, and b & c are the chemical structures of the dyes Z907 and N719, respectively. Figures adapted from ref. 25 with permission from the American Chemical Society.

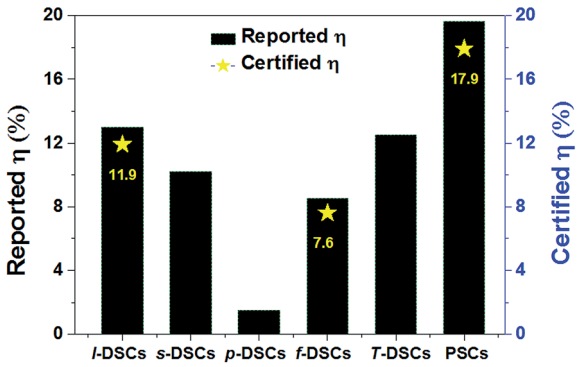

Fig. 3 Efficiency comparison of various types of DSCs. The stars show certified efficiency values of corresponding devices. The confirmed η for various devices is reported in ref. 9.

promising; however, their performance is limited due to the low voltage of p-type photocathodes.[31] A breakthrough in the third generation solar cells is the emergence of perovskite-sensitized solid state solar cells (PSCs), which employ an organic–inorganic hybrid perovskite absorber (commonly $CH_3NH_3PbX_3$, X = Br, Cl, or I) on a very thin MOS layer (<1 μm).[32–37] Although PSCs initially emerged as a class of DSCs, they are likely to be considered a new class of solar cells. Confirmed η values as high as ~17.9% have been reported in PSCs, which represents a four-fold improvement in just four years since the first report.[9] These PSCs are another emerging area; nevertheless, the replacement of lead (Pb) with some non-toxic material may presumably increase their market acceptability.[38] Results on the scalable fabrication of PSCs have recently been reported across the globe, with η values reaching 8.7%.[39,40]

3. DSCs *versus* other PV technologies

One of the major drawbacks of conventional silicon PV technology is the amount of solar irradiation required for its start-up operation (200–300 watt per m^2); this amount increases to 800–900 watt per m^2 for peak performance.[41] Despite the fact that the certified η in DSMs (8.2%)[76] is far lower than that achieved in the first two generation solar cells (~15–20%), their working capability in low light conditions and transparency place them at the forefront for applications such as BIPVs. This exclusive feature of DSMs not only increases their operating hours, but also allows them to be deployed in shaded regions, corners or bends in buildings. A comparative study by Dyesol Ltd. revealed that DSMs deliver 65–300% higher power output on cloudy days compared to silicon and thin film solar cells (Fig. 4a and b).[42] Their analysis revealed that the performance of DSMs is higher on days when the solar irradiance is <300 kW m^{-2}. In another six month comparative study by Aisin Seiki CO. Ltd.,[43] DSMs (64 cell modules of size 10 × 10 cm^2) showed 10% increased performance on a hot sunny day and 20% increased performance on a cloudy day compared to single crystalline Si-modules. The study also demonstrated that DSMs perform better in midmorning and midevening, widening their available performing hours. A similar performance was demonstrated in Japan in a world solar car rally (July 2008); 2 × 8 m^2 DSMs (developed by Taiyo Yuden Co. Ltd.) were deployed on a test race car and achieved a speed of 11.8 km h^{-1} in cloudy weather, a speed similar to the 12.5 km h^{-1} achieved in sunny weather.[43] These reports highlight the exclusive features of DSMs and their capability to work in low light conditions to overcome the limitations of conventional PV technology. Moreover, a recent study by Zardetto *et al.*[44] showed that when turned into a curved shape, DSMs on flexible substrates outperform flat devices, further strengthening their potential application diversity. The study reported ~10% higher power output in the flexible device built on a metallic substrate compared to a flat one when normalised to their footprint. These results are encouraging for the potential applications of DSMs in low light areas and conditions. For example, in zero energy buildings, DSMs can be deployed as smart windows to simultaneously add to the aesthetic quality while producing solar electricity for almost the entire day.

Unlike the first two generation solar cells, which require clean rooms and vacuum-based device fabrication facilities, DSMs can be fabricated in less demanding conditions. To further ease their fabrication, researchers have successfully demonstrated low temperature (<150 °C), binder-free coating

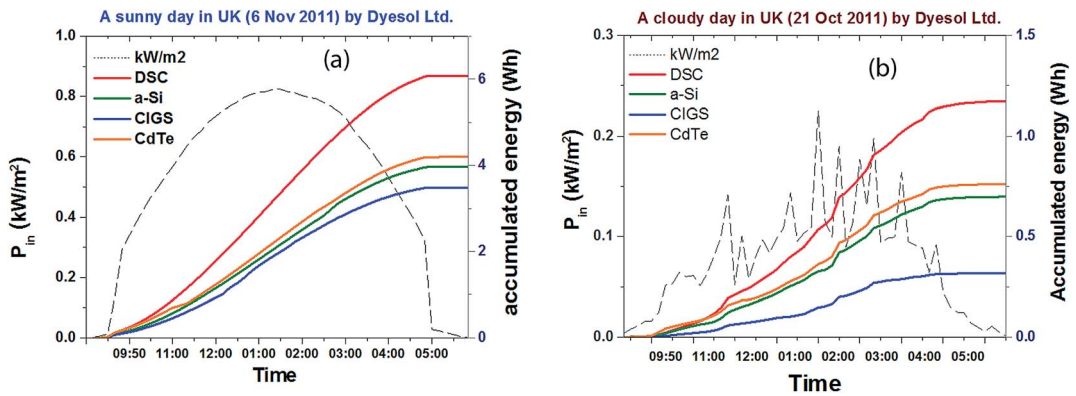

Fig. 4 Performance comparison of DSCs with other photovoltaic technologies on (a) a sunny day and (b) a cloudy day (data courtesy of Dr Damion Milliken of Dyesol Ltd.).

processes on plastic substrates, reporting η values as high as ~8% for single cells[27] and ~3–4.5% for DSMs.[45,46]

The performance of DSCs improves from room temperature to ~40 °C (ref. 47) because electrolyte viscosity decreases with increasing temperature, which meliorates the ionic transport inside the MOS.[48,49] Conversely, the performance of silicon-based solar cells drops at elevated temperatures as the dark recombination current increases with temperature.[50,51]

3.1 Manufacturing cost of DSMs

In addition to the applicability of DSMs in low-light and flexible conditions, their deployability strongly depends on the module manufacturing cost and associated economics. Table 1 shows a comparison of manufacturing costs normalised with respect to the peak output power compiled from various sources. Kalowekamo *et al.*[52] estimated the manufacturing cost for DSMs and compared it with first two generation solar cells. In their study, the estimated DSM cost varies from 0.5$/$W_P$ ($\eta \sim 5\%$) to 1$/$W_P$ ($\eta \sim 15\%$). The DSMs provide solar electricity at a cost significantly cheaper than the first two generations of solar cells (Table 1). Fujikura Ltd., a DSM manufacturer, reports that the manufacturing cost can be reduced to 0.4$/$W_P$ provided that an annual production level of 100 MW is achieved.[53] The lower cost of DSMs can be attributed to the cheaper material cost and easy fabrication. In addition, the photoelectrode MOSs such as TiO_2, ZnO, and SnO_2 are very abundant, unlike indium, which is used in some of the thin film solar cells.[4]

The major contribution (50–60%) to the manufacturing cost of DSMs arises primarily from dyes, electrolyte, and substrates.[57,59] The materials for DSMs are still produced on a research scale; the cost would be significantly reduced for commercial scale production.

Fig. 5 shows manufacturing cost data for a series of monolithic DSMs (90 cm × 60 cm, power output 50 W_P m^{-2}). These statistics were compiled by one of the world's leading DSM developers, Solaronix Ltd., for an annual production of ~20 MW_P per year.[59] The DSM manufacturing cost was estimated to be ~0.97 Euro/W_P for $\eta \sim 7\%$ and process output yield ~90%. Notably, two thirds of the total cost arose from materials: dyes and electrolytes contributed one third, sealing and

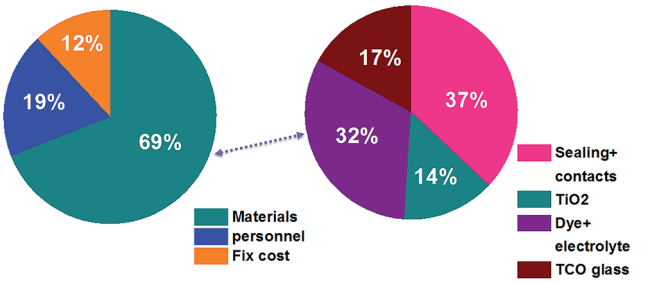

Fig. 5 Estimation of the projected share to overall cost during large scale manufacturing (left panel) and the cost for various materials used to fabricate 20-MW DSMs (right panel). Data taken from ref. 59.

interconnections cost more than one third (37%), and substrates cost ~17% of the material cost (~22%, ~25% and ~12% of the total cost, respectively). As suggested by Hashmi *et al.*,[57] a substantial reduction in this price is possible by replacing some of the expensive material components (*i.e.*, replacing glass with plastic will reduce substrates cost by one third, although one must consider the additional costs of additional barrier layers). Replacing FTO by stainless steel sheets can save up to 80% of the substrate cost (9% of the total cost). Similarly, although s-DSCs offer fewer sealing difficulties than l-DSCs, they are still vulnerable to moisture and oxygen permeation.

4. Dye-solar modules: from laboratory to commercial development

After the single cell η was reported in 1991, the same group reported the first DSMs in 1996.[60] In their module, six DSCs with areas of ~3.3 cm^2 were serially connected on an FTO substrate to achieve an η of ~5.3%. Since then, a number of studies worldwide have reported the development of various types of DSMs with various designs including series, parallel or their combination. A survey of the literature shows that efforts in the development of DSMs are rather unimpressive; only one research paper on DSMs is published for each hundred papers on laboratory devices. Fig. 6a shows a summary of research

Table 1 Cost/W_P and η comparison of various types of solar cells/modules; the values are taken from ref. 28 unless stated otherwise. Certified efficiencies are marked with a '*'. * Market prices of silicon panels have dropped in recent years to as low as ~0.7$/$W_p$; however, such prices are from few producers, and the practicality and sustainability of such prices are yet to be determined (http://www.nyse.com)

Device	η in cells (%)	η in modules (%)	Module manufacturing cost/W_p ($)
Multijunction (III–V)	44.7* (FhG-ISE)	—	—
Si	24.7 (UNSW)	14.5 (ref. 54)	~0.7*–1.29 (ref. 55)
CIGS	19.8* (NREL)	18.7* (FhG-ISE)	1.13 (ref. 55)
Si (amorphous)	10.1* (AIST)	—	—
CdTe	17.3* (NREL, ref. 55)	11.7	0.74
Organic PVs	10 (ref. 55)	6.8*	0.75–2 (ref. 56)
Dye solar cells	11.9* (SHARP)	8.2* (SHARP)	0.5–0.94 (ref. 52 and 57)
Perovskite solar cells	17.9*[9]	8.7 (Planar structure)% (ref. 40) 5.1% (Monolithic modules)[39]	NA
QDSCs	7 (ref. 58)	Not developed yet	NA

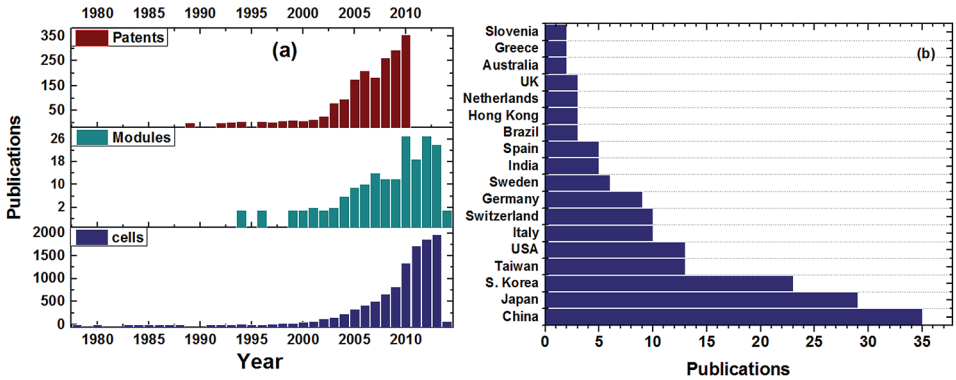

Fig. 6 (a) Research trends in DSCs: papers published on single cells (bottom panel); publications on DSMs (middle panel); and patents registered globally (top panel; data is taken from ref. 61). (b) Trends show the affiliation of various countries working on large area development of DSCs. Data is taken from Scopus in January, 2014 using the keywords 'dye-sensitized solar modules' and 'large area dye-sensitized solar cells'.

papers and patents published on DSCs and DSMs. A study on the involvement of different countries in DSMs was also made and is shown in Fig. 6b; one can see that, in order of descending contribution, China, Japan, Korea, Taiwan and the USA are the leaders in DSM fabrication.

4.1 Dye-solar cell/modules as electrochromic windows

For residential and commercial users, a significant portion (10–30%) of the peak electricity demand arises from overheating caused by glass windows that allow heat radiation to enter a building.[62] This share can be reduced by (i) controlling the optical transparency of the windows to block heat radiation from entering the buildings and (ii) converting the passive windows into smart windows that can harvest the solar light into electricity.[63–65] Towards the second strategy, an energy storage smart window, also called an electrochromic device (ECD), that simultaneously harvests and stores solar energy by integrating two electrochemical devices (DSCs and supercapacitors) has been developed.[66,67] The ECD can be divided into two parts: photovoltaic and EC components separated by an ionic conductor with negligible electronic conductivity to avoid short circuits between them. Such devices are self-powered, unlike the conventional ECD windows, which need an energy supply for operation. The window changes from a bleached to a coloured state due to the reversible reaction in the electrolyte upon light absorption.[68]

Self-powered switchable devices can be made in two ways: (i) photoelectrochromic window (PECW), which changes its transmittance using the electrical output of the DSC to block heat radiation (Fig. 7);[69] and (ii) smart energy storage window, where the primary concern is to produce electricity and store it in an integrated supercapacitor.[66] The primary requirement for PECWs is an electrochemical material that changes its transmittance with applied potential. Various metal oxides (WO_3, NiO, IrO_2, and Nb_2O_5) and polymers such as polyaniline and poly(3,4-ethylene-dioxythiophene) have been employed as EC materials.[70–73] In a recent study, Yang *et al.*[69] reported a lowering of transmittance from 47 to 9% upon electrochemical reaction employing PECW ($\eta \sim 1.2\%$). In another study, an η of up to ~2% was reported for an Al-doped boron oxide-based PECW due to the conductivity of the dopant used.[74]

As the self-powered switchable devices need to be highly transparent, the films should be made very thin. These devices usually consist of three sequentially coated layers and require precise fabrication to avoid short circuit.[76,77] Thin silicon solar modules are commercially available as switchable windows with $\eta \sim 5\%$;[78] however, DSC-based ECDs are still in the laboratory stage. There are rare reports on employing T-DSCs as switchable or smart windows; however, the work is still at the laboratory scale.[79]

4.2 Emergence of dye-solar module businesses

DSMs have now reached a level of deployment as a photovoltaic device. Table 2 shows a list of industrial sectors that have emerged to develop this photovoltaic technology, their inferred core business and key achievements. Owing to the transparency

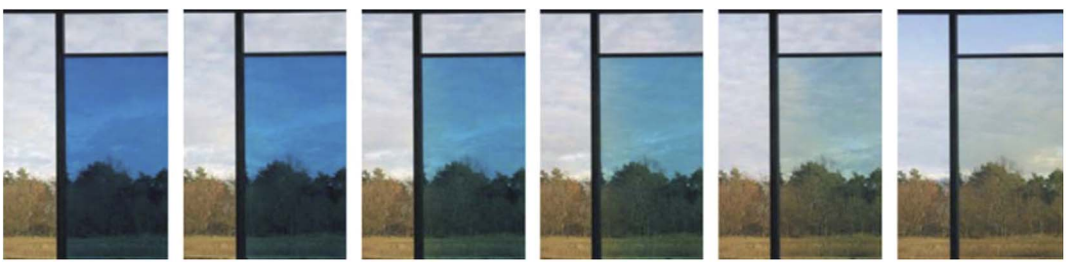

Fig. 7 Switching sequence of an ECW. Figure adapted from ref. 75.

Table 2 Global commercial companies that develop dye-solar cells/modules. The information is inferred from their websites/published reports on websites and (ref. 43), unless stated otherwise

No	Company	Affiliation	Core business	Major achievements in DSCs
1	S Samsung SDI	Korea	Electronic devices such as LCDs, mobile phones, and more recently, energy storage and harvesting devices	Dye solar panels for BIPVs, smart windows with integrated storage, tandem DSPs
2	SHARP	Japan	Electronic products	Certified η of 11.9% in single cells by tuning haze effect, certified highest module PCE (8.2%) in W-type module, cost effective back contact DSCs ($\eta \sim 7.1\%$) with only one substrate, 8.1% efficient quasi-s-DSCs employing a polymer electrolyte
3	G24 Power	UK	Solar power, especially third generation PVs	Started DSC plant in 2007 (18 000 sq. ft), flexible waterproof bags, commercial applications for indoor electronics, roll-to-roll processing capability of 800 m in ~3 h, specialized in indoor electronics such as key-boards, mouses, e-book covers, solar bags, MP3 players, *etc.*
4	Konarka	USA	Spinoff company of MIT for DSCs	Licensed its DSC IP to G24
5	Dyesol	Australia	DSCs materials and commercial development	DSMs, BIPVs, integration of DSCs in roof materials (in process), s-DSMs and f-DSMs. Developing DSMs and s-DSMs
6	Solaronix	Switzerland	DSC material and commercial development	Panels with an active area of ~200 m^2 are shipped to EFPL with an estimated annual production of 2000 kW h. Developing DSMs and materials for solar cells/modules
7	Dynamo	Sweden	DSCs materials and commercial development	Preparing co-based electrolytes and porphyrin dyes
8	Oxford PVs	UK	s-DSMs, PSMs	Currently working on perovskite solar modules
9	Dyepower	Italy	Development of DSMs for BIPV and facades applications	Running an automated pilot line for the production of A4 size DSMs and for larger area strings/panels. UV, humidity-freeze and damp-heat IEC 61646 stability tests successfully passed on A4 size modules
10	EFPL	Switzerland	Organic PVs, materials and characterisation	Held the main patent on mesoporous dye solar cell structure. Highest uncertified η in DSCs (13%), one of the highest η in perovskite-based solar cells (15%), the first report on DSMs in 1996 (monolithic series modules (10 × 10 cm^2) with $\eta \sim 6\%$

Table 2 (*Contd.*)

No	Company	Affiliation	Core business	Major achievements in DSCs
11	Fujikura	Japan	Optical fibres	Developing DSCs for both outdoor applications and indoor electronics such as mobile phones, testing ionic liquids and gel-electrolytes in modules, thermal stability and outdoor testing of more than 200 sub-modules (20 cm^2), modules passed IEC 61646 (stability test)
12	3G Solar	Israel	DSC technology	Installed DSC mini modules to charge computer peripherals, surveillance cameras, electronic bracelets and medical devices
13	CSIRO	Australia	Research agency	Colourful and transparent DSMs for BIPVs, materials for cost-effective DSCs
14	Taiyo Yuden Co. Ltd.	Japan	Electronic components	Flexible DSC using Ti foil as counter electrode for a sub-module of 15 × 15 cm^2 (0.3 mm thin), tested race car using 2 × 8 m^2 connected sub-modules in world solar car rally in 2008 and achieved a speed of 11.8 km h^{-1} in cloudy weather, similar to the 12.5 km h^{-1} achieved in sunny weather
15	SONY Technology Centre	Japan	Electrical appliances	Started research on DSCs in 2001, applications for terrestrial power and indoor electronics, achieved 11.1% confirmed η in 2009 (APL, 94(073308)), "Hana-akari", a solar lamp powered by DSCs, developed
16	Shimane Institute of Technology	Japan	Governmental organization	J2 dye, large area DSC (1.25 m × 0.75 m) developments and stability testing for 1000 h at 80 °C, 'EneLEAF' in collaboration with Nissha. Ltd.
17	Toyota/Aisen Seiki	Japan	Components and systems for automotive industry	One of the earlier R&D industries to work on DSMs, S-type monolithic connections, stability tests in outdoor exposure in 2006 for 2.5 years
18	Peccell Technologies, Inc.	Japan	Venture company of Toin University of Yokohama	Plastic modules of DSCs, 4 V in a serially connected module of 10 × 10 cm^2, the world's largest fully developed plastic module (0.8 × 2.1 m) is the lightest DSM weight (800 g m^{-2}) with a capability of providing >1000 V
19	Eneos Co. Ltd.	Japan	Iol company but established a joint sub company named as 'Sanyo Eneos solar co. Ltd.'	Bi-layer photoanodes, solid state DSMs (10 × 10 cm^2)

Table 2 (*Contd.*)

No	Company	Affiliation	Core business	Major achievements in DSCs
20	NGK Spark Plug Co., Ltd.	Japan	Spark plugs	Started DSC research in 2003, adopted lithography in monolithic module fabrication, founder of ball grid DSC structures, which replace Pt for catalysis purposes and utilize 95% active area
21	ITRI Taiwan (Industrial Tech. Research Inst. Of Taiwan)	Taiwan	Applied research and technical services	Transferred technology to Formosa Plastics and mass production is expected in 2015
22	Mitsubishi Paper Mills	Japan	Paper, pulp, and photosensitive materials	D-series dyes or indoline dyes perform better with ZnO due to metal free nature
23	Panasonic Denko Co. Ltd.	Japan	Branch company of Panasonic, electronic appliances	See-through modules for indoor applications, stability testing and encapsulation to prevent electrolyte leaking, use of K9 dye instead N719 to improve stability
24	KIST (Korean Ins. Of Sc. and Tech.)		Materials for DSCs and device development	Flexible DSCs, especially stainless steel-based devices with $\eta \sim 4.2\%$ higher than plastic based DSCs, molecular engineering helped in achieving an PCE of 11% at their labs, the technology is transferred to Dongjin Semichem Ltd.
25	J Touch Taiwan	Taiwan	Touch panel solutions	Started using DSCs in indoor electronics such as portable time clocks
26	Fraunhofer ISE	Germany	Environmentally friendly energy harvesting and storage research	Scalable development and stability research on DSMs, first large area (30×30 cm^2) glass frit-based module design with thermal stability testing up to 80 °C
27	Institute of Plasma Physics (CAS, China)	China	Utilisation of fusion energy	A 500 W DSC power station was installed in 2004 with $\eta \sim 5.9\%$ in parallel modules, research focused on photoanode optimization, device packaging and interconnections
28	ECN (Energy Research Center of the Netherlands)	Netherlands	Energy research institute	First EU lab for DSC development started in 1995, stability tests for 1000 and 10 000 h, introduced master plate design, installed semi-automated DSC manufacturing up to 100 cm^2
29	Gunze Ltd.	Japan	Electronic components and garments	Wearable DSC, a unique application (28 cells with required electronics are attached to a jacket and used as mobile charge)
30	Yingkou OPV Tech New Energy Co., Ltd.	China	Upscaling DSCs/DSMs	Colourful, artistic and transparent DSMs in the form of glass windows and

Table 2 (*Contd.*)

No	Company	Affiliation	Core business	Major achievements in DSCs
				screens. Flexible and portable DSMs are also manufactured and available for commercial use
31	Ricoh	Japan	Electronic (imaging and printing devices, for example)	s-DSMs for indoor lighting
32	Merck	Germany	Chemicals and pharmaceuticals	Electrolytes for DSCs, precursors for various photoanode materials
33	Acrosol	Korea	Research & development, solar panel manufacturer	N/A
34	NLAB Solar (name changed to Exeger)	Sweden	Industrial production of DSMs	Pilot plant installed for the production of DSMs as BIPVs and AIPVs
35	Dye Tec Solar (Dyesol-Pilkington JV)	USA/Global	DSMs in BIPVs	Joint venture of Dye-sol and Pilkington
36	Tata Steel Europe	India	Steel roofing	Joint venture of Dye-sol and Tata Steel

of DSCs and their excellent performance in low levels of light, the potential key venues for installing DSCs are indoor electronic applications and BIPVs (Fig. 8a–d),[80] as their efficiency *vs.* transparency performance can be tuned.[17] DSCs work well in diffused or low light and are less affected by the angle of incidence, with efficiencies that increase with angle of light incidence (up to ~50°) by ~10–16%.[81] Moreover, BIPVs have an advantage over centralized solar power generation because the electricity generated is consumed in place, avoiding transmission line losses and infrastructure costs. DSMs with active areas of ~200 m^2 were installed as windows of a green building in April, 2014 at the École Polytechnique Fédérale De Lausanne (EFPL) campus, Switzerland (Fig. 8a and b).[82] These panels are estimated to be able to generate ~2000 kW h of annual solar electricity. The transparent panels are in five different colours (representing a desirable unique feature of DSCs) and were developed by Solaronix. This massive production is an important milestone for the commercial deployment of DSCs, although a number of issues including the lifetime of these panels under operating conditions are yet to be fully addressed.

Dyesol, another leading DSC company, has recently launched projects on the integration of DSCs into buildings with their various industrial partners (Tata Steel Europe of UK, Pilkington North America of USA, Timo Technologies of South Korea) and on DSC-powered combined energy generation and storage (CEGS) devices.[83] These projects are expected to further reduce the cost/kW h as double-coated glass windows in the buildings meant for UV protection and antireflective coatings are used as substrates for DSMs. Oxford Photovoltaics, a spin-off company of Oxford University, is working on all solid state perovskite based modules (PSMs). However, the lifetime of the solid state PSMs under outdoor conditions is yet to be determined.

5. Current research on dye solar modules

Several major advancements have been made to upscale DSMs in terms of their various interconnection designs, material components, scalable fabrication processes, outdoor stability testing, tandem cells/modules to absorb a wider range of light over the solar spectrum, and innovative applications such as a hybrid energy harvesting and storage devices. These advancements are paving the way towards the ultimate goals of this technology: successful commercial deployment as a fossil fuel alternative and cost-effective competition with the incumbent photovoltaics. Many developments have been seen in the scalable production of DSMs such as the fabrication of modules with certified η values of up to 8.2%,[84] the emergence of s-DSCs and s-DSMs to enhance device lifetimes,[85–87] the initiation of flexible DSMs and their low temperature processing,[44,46] long term stability and thermal testing of transparent conducting oxide (TCO)-based DSCs up to 80 °C,[81,119] and their application as smart windows.[88,89] Recent achievements such as the first commercial large scale delivery of DSMs from Solaronix, high efficiency s-DSMs from Dyesol (reported $\eta \sim 11.3\%$ at 1 sun, results are yet to be published),[90] and thermal stability testing up to 90 °C have made further progress towards the successful commercial production of DSMs.[91] Fig. 9 shows a timeline of DSM development since their first report in 1996. It highlights the major achievements in DSM development and also projects their future progress. In this section, we briefly review various developments in DSM fabrication techniques and designs.

5.1 Fabrication processes of dye-solar modules

The fabrication of DSMs differs from that of single cells primarily due to the electrical connections among neighbouring

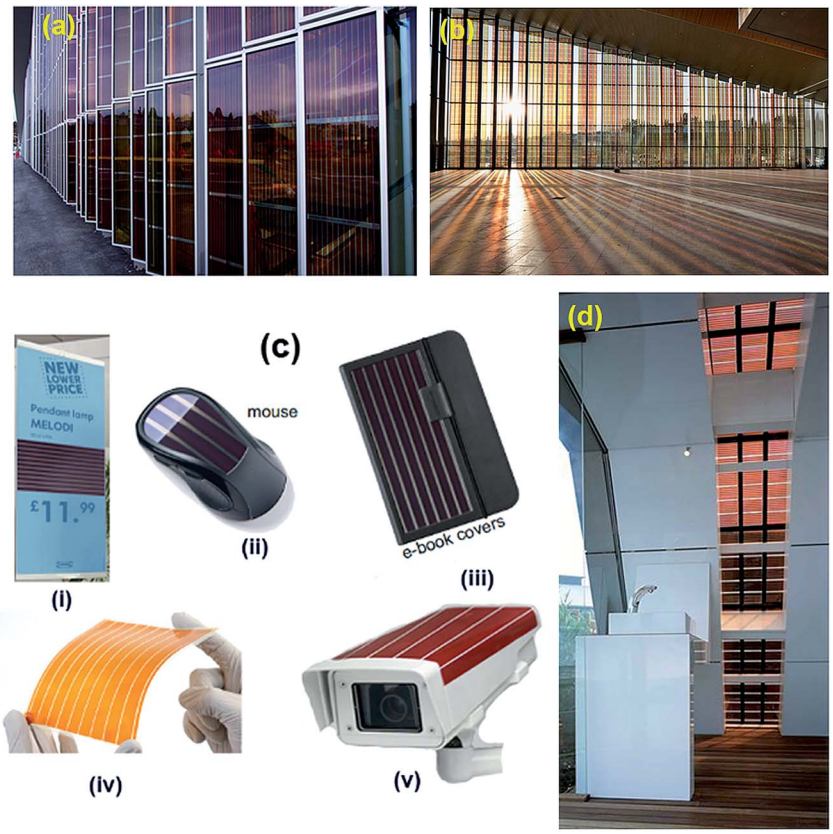

Fig. 8 (a and b) DSM installation recently completed at the EFPL campus (photos are courtesy of David Martineau of Solaronix Ltd.), (c) images of few commercial DSC products on the market (i–iii) are indoor electronics by G24, while iv and v are developed by 3G Solar, and (d) DSMs installed as the interior of a washroom by Dyesol Ltd. (image courtesy of Dr Damion Milliken of Dyesol Ltd.).

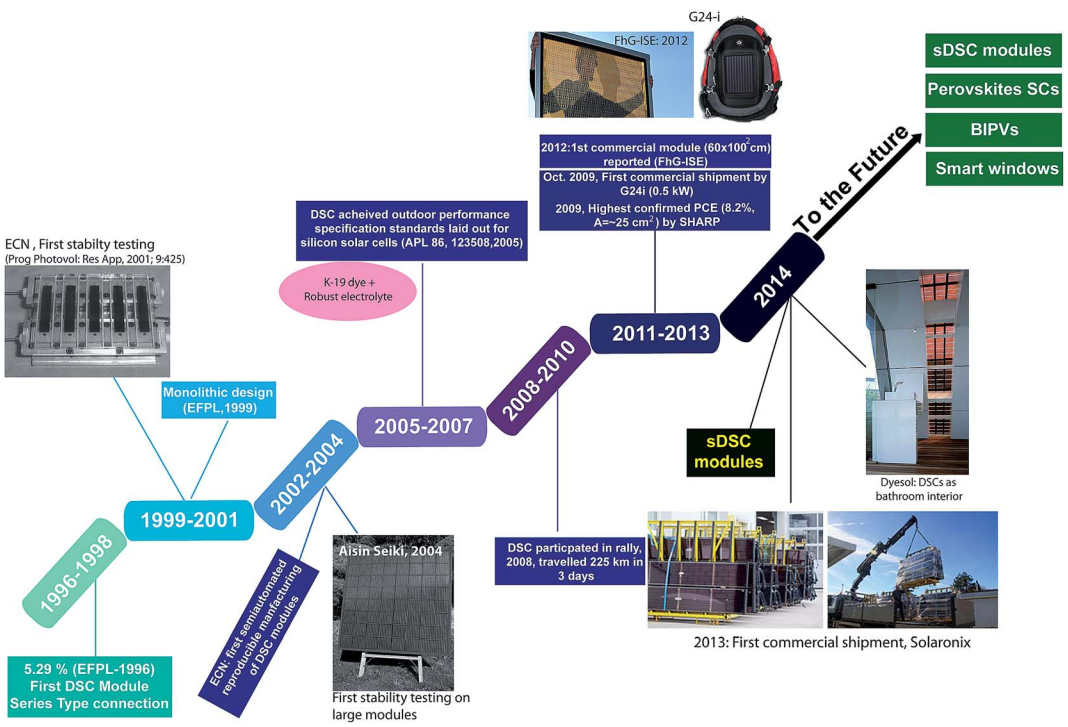

Fig. 9 Step-by-step historical evaluation of dye-sensitized solar modules.

cells. Screen printing is usually employed as a coating method for the photoanodes of DSMs[92,93] as it permits the facile and controlled deposition in the few to 20 μm thickness range and is also compatible with roll-to-roll processing. In addition, this technique offers compactness and good adhesion of TiO_2 with the substrates, which otherwise often peels off from the surface upon annealing. Screen printing technology is a commercially available printing method and can be used for printing on both glass and plastic substrates. Fig. 10 shows a block diagram of various processes involved in DSM fabrication. For details of each section, we refer the reader to the pioneering work of Späth *et al.*[94] and a recent review by Hashmi *et al.*[57]

The working and pre-drilled counter electrodes are cleaned using trichloroethylene, acetone and ethanol. The electrodes are then etched for series connections. CEs are platinized by depositing Pt precursor pastes and then cured in a furnace. TiO_2 layers are coated on the working electrode (WE) *via* screen printing to obtain the desired photoanode thickness (~10 μm). A heat treatment (100 °C) after each coating cycle is helpful to stabilise each layer. In a batch process, the coated FTOs are heated on a belt furnace to remove organic binders in the paste and to sinter TiO_2 nanoparticles together. Interconnections (series) or current collecting fingers (parallel) between neighbouring cells are made using conducting media (such as silver). The WEs are sensitized with a dye, and the device is completed by placing the patterned CEs on the WEs separated with a 30–60 μm thick spacer and sealing. The Ag patterns are encapsulated to avoid their contact with the liquid electrolyte. The electrolyte is filled through drilled holes, and the holes are sealed *via* cover slips and sealant material after filling.

The typical dye-sensitisation methods are not suitable for DSM batch production as it requires longer soaking hours. Accelerated dye-sensitization processes are introduced, requiring a few minutes for dye-anchoring and yielding similar photovoltaic performances to that of typical overnight soaking. Such accelerated methods may reduce the batch production time significantly. ECN researchers introduced a novel dye-anchoring method where they pumped the dye solution in a pre-sealed DSM through two drilled holes.[95] Such a method is beneficial when the device is to be sealed using a glass frit that requires high temperature (~500 °C) for adhesion because the dye decomposes at such a temperature. During DSM fabrication, encapsulation and electrolyte filling are amongst the crucial steps. Good encapsulation is crucial for long lifetimes, and improper filling leads to significant performance degradation for similar devices. At present, many researchers use pre-drilled holes at the CE to inject the electrolyte *via* vacuum filling. This process, however, is tedious, and a number of automated units for electrolyte filling are now offered by various companies such as Dyesol Ltd. to ease the continuous production of DSMs.

5.2 Design configurations of dye-solar modules

After intensive research for nearly two decades, commercial DSM developments are underway (Table 2). The fabrication of DSMs is different from a laboratory scale device due to (i) large scale metal oxide coating on TCOs, (ii) extensively impermeable sealing to humidity and air as well as to prevent liquid electrolyte from drying and leaking, (iii) electrolyte filling, (iv) interconnection for modules (series or parallel) and external electrical connections, and (v) most importantly, the anticipated lifetime of the device compared to that offered by silicon based devices (~20 years). Electrical connections need intensive care during the fabrication process as an ineffective contact will ultimately lower FF by adding to the series resistance and eventually lowering the η.[98,99] Two major types of connections are employed for DSMs fabrications: (i) parallel designs, which provide high photocurrent, such as parallel grid connections; and (ii) series designs for high output voltage including Z-type, W-type, and monolithic connections. These designs employ large rectangular strips (area ≥3 cm^2) interconnected serially or in parallel (Fig. 11a–e). Other types of connections such as master plate design and ball-grid connection have been reported by a few researchers.[128,129]

In this section, we highlight the differences in these various interconnections along with their advantages and disadvantages and also critically analyse their photovoltaic performances. For convenience, we define three common terms (active area, aperture area, and total area) that will be used extensively in this article: active area is the area covered by only the TiO_2 strips on a substrate; aperture area is the sum of active area and the region between the cells (which are occupied by the sealants, interconnections or collecting grids); and total area is the total substrate area that also includes the peripheral area used for bus bars and blank spaces on the substrate.

5.2.1 Series connections

i. Monolithic design (S-type). Here, the term monolithic refers to the sequential deposition of electrode material layers by successively pasting and pressing them. The monolithic DSMs are attractive as they are made on a single substrate

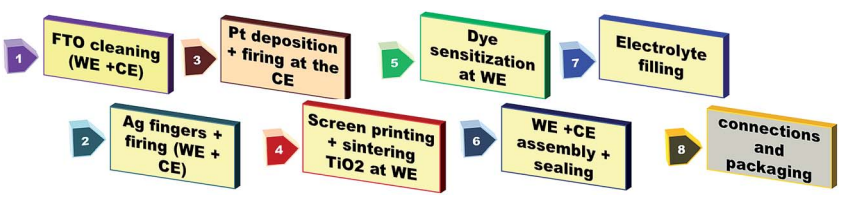

Fig. 10 A schematic of a parallel DSM assembly line. The figure is drawn based on the ref. 96 and 97 which outline the steps for parallel modules. For series-connected modules, the FTO has to be scribed for cell isolation. The W-type modules requires no Ag interconnections, and for the Z architecture, the order of the steps can change. For more detail on the fabrication of series modules, refer to ref. 96 and 98.

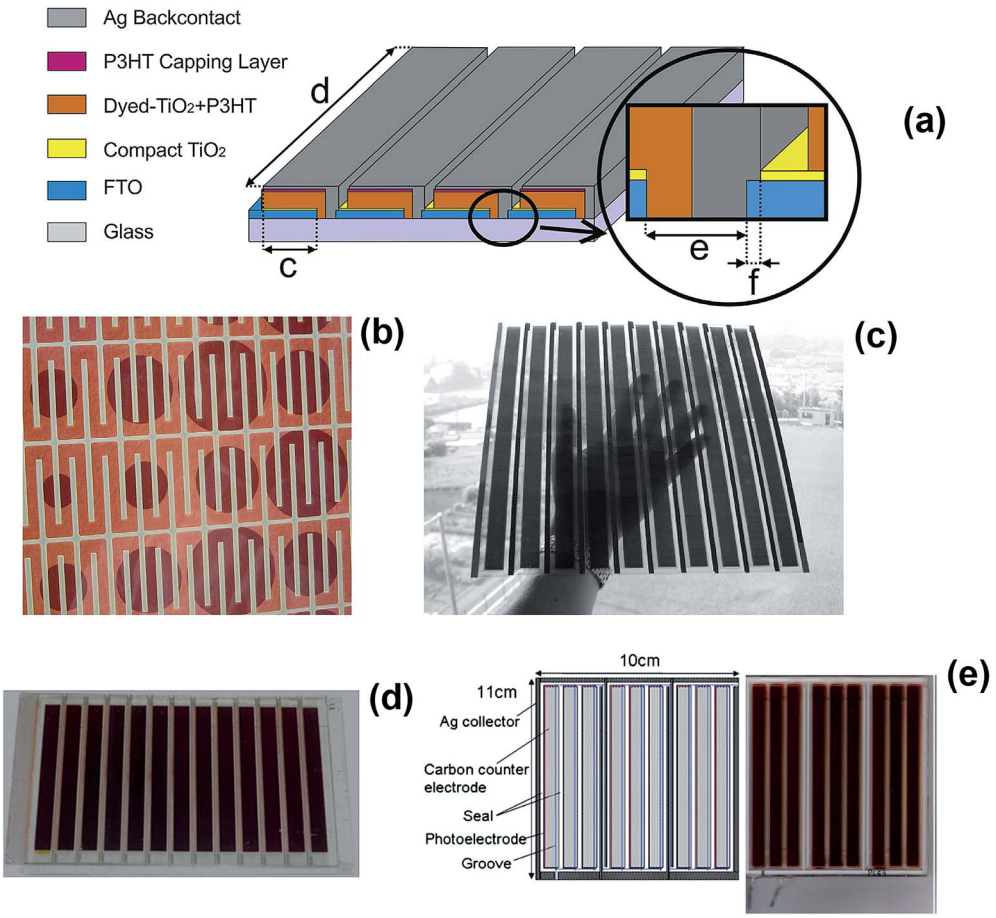

Fig. 11 Some commonly adopted designs of conventional DSMs. (a) Design schematic of a DSM employing P3HT (poly(3-hexylthiophene-2,5-diyl)) as a hole transport medium,[87] (b) DSM design for façade application under the European project COMSOL,[100] (c) a flexible plastic DSM,[101] (d) a series Z-type module,[102] and (e) a parallel grid type design where the individual strips are surrounded by a metallic current collector.[103] Other common architectures involve the W-type and monolithic designs for series connected DSMs (not shown).

(Fig. 12a) and eliminate the need for the CE. Owing to their single substrate architecture, monolithic designs are highly compatible with roll-to-roll processing of flexible DSMs as they do not require continuous photoanode thickness.[104] The fact that the device is fabricated layer-by-layer, rather than by assembling two electrodes together, makes this design more tolerant to substrate non-planarity. These designs also replace expensive platinum by cheaper carbon black as the CE; therefore, 20–30% of material cost reduction is estimated for monolithic-type series module designs compared to other designs.[105]

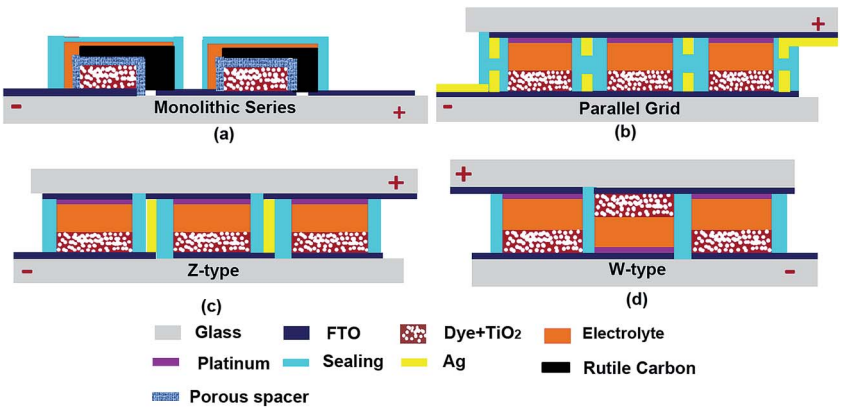

Fig. 12 Schematic of different types of series connections: (a) monolithic, (b) parallel grid, (c) Z-type and (d) W-type.

Monolithic design is also called Kay cell, named after the inventor Andreas Kay, who reported the first DSM in 1996 with $\eta \sim 5.3\%$.[60] The notable achievements in their report are (i) the replacement of expensive platinum with porous carbon as CE, (ii) a porous insulating layer between the WE and CE to avoid short circuit while allowing the electrolyte to freely diffuse through its pores, and (iii) a continuous, conveyerised fabrication process of series connected DSMs. The thickness of the photoanode in the Kay cell was ~80 μm (TiO_2 10 μm, Rutile spacer 10 μm, & carbon black 60 μm). The DSMs (six strips of 4.7 × 0.7 cm^2 with total area ~21 cm^2) yielded $\eta \sim 5.3\%$ ($V_{OC} \sim 3.90$ V, $I_{SC} \sim 28.55$ mA, & FF ~ 0.61). The major drawbacks of this design are a much lower J_{SC} (1.3 mA cm^{-2}) despite a high output voltage (~4 V), high opacity and poor sealing of the device. ZrO_2 has also been employed to replace the opaque rutile spacer; however, the transparency was lower than that of a conventional Pt electrode.[104]

Since the first report on series interconnections, there has been no significant progress in these designs. Thirteen years after the work of Kay in 1996, the improved transparency of the monolithic designs was reported by AISIN SEIKI.[106] They replaced (i) the opaque counter CE material (carbon black) by a highly transparent paste comprising In_2O_3:Sn and Pt nanoparticles and (ii) the opaque rutile spacer by SiO_2 (refractive index 1.5, close to that of the electrolyte used), thereby considerably improving the transparency. The photovoltaic performance of their module was rather inferior compared to the first report; the four-fold larger modules developed by AISIN SEIKI (95 mm × 95 mm, area ~ 91 cm^2) resulted in 30% greater J_{SC} (~1.7 mA cm^{-2}) compared to Kay's first design (area ~ 21 cm^2). The lower J_{SC} limited the η to <3% despite a higher output voltage (~8 V).

Monolithic DSMs are built on a single substrate (WE only) and are therefore known as a cost effective design. Another major advantage of this design is the high active to total area ratio. In both reports on monolithic designs, this ratio was >90%. However, these connections result in lower J_{SC} due to high series resistance and low FF ($\leq$0.6).[106,107] As the individual strips are connected in series, immense attention is to be given to match the J_{SC} in all individual cells. Due to the type of series connection, the final J_{SC} is lowest in the serially connected cells. Monolithic transparent DSMs on a single substrate with high transparency have yet to be reported.

ii. Z-type and W-type interconnections. Both of these types are series connected devices: one of them uses a vertical metallic conductor to connect the neighbouring cells (Z-type), whereas the other (W-type) does not require it (Fig. 12c and d). The names 'Z-type' and 'W-type' stem from their resemblance to the letters 'Z' and 'W', respectively. The Z-type connection, also called Z-contact, is adopted from thin film solar cells.[104] In this design, the individual cells are serially interconnected *via* a conducting medium (usually silver) so that the CE of the first cell is connected to the WE of neighbouring cell and *vice versa* (Fig. 12c).

The first Z-type DSM was demonstrated in 2004 by Toyoda *et al.*,[108] who connected 64 DSMs (10 × 10 cm^2) in series to form a large panel. The researchers carried out the first long term stability testing of DSMs for six months and compared their performance with a crystalline silicon module of similar output power rating. Although the photovoltaic parameters of the DSMs were not exclusively reported, the DSMs showed a 10–20% greater power output over a period of six months. The major issue reported during fabrication is the hermetic sealing of the DSMs, resulting in performance degradation. This issue is resolved in a subsequent report by Sastrawan *et al.*,[95] who introduced a highly stable glass frit as a sealant. As the frit is processed at a high temperature (>500 °C) at which the dye decomposes, a novel pumping method for dye anchoring was employed. The dye was pumped *via* two holes after the sealing of DSMs of a total area up to 30 × 30 cm^2. The DSMs resulted in an η of ~3.5% ($V_{OC} \sim 20$ V, $I_{SC} \sim 168$ mA, & FF ~ 0.53) with an active area of ~680 cm^2 (74% of total area). The major drawbacks of these reports are the low FF (<0.55) and low J_{SC} (<0.5 mA cm^{-2}) arising from the high series resistance of the photoelectrodes. Jun *et al.*[107] reported a DSM (10 × 10 cm^2) with significantly superior performance, *i.e.*, $\eta \sim 6.6\%$ ($V_{OC} \sim 8$ V, $J_{SC} \sim 1.23$ mA cm^{-2}, & FF ~ 0.67). The significant enhancement in FF and J_{SC} was achieved by restricting the width of each individual strip (<1 cm). A similar advancement was reported by Giordano *et al.*,[102] who optimised the geometry of the photoelectrode using a back reflector to achieve an η of up to ~7% on the aperture area in modules with areas of ~45 cm^2.

Despite the high voltage achieved by Z-type DSMs, they can suffer from relatively low active areas due to the vertical connections and surrounding seals, the complexity of fabrication and the additional series resistance produced by added interconnection, which can reduce the fill factors. Furthermore, the silver interconnects corrode easily in the presence of liquid electrolytes. In an innovative design by Dyesol, the silver is replaced by a less corrosive material (45 μm titanium particles and 5 μm tungsten particles in a polymer matrix).[109] Although the vertical connections are presumably less conductive than Ag per unit section, in addition to adding stability to the device, this design also eliminated some additional sealing required in the Z-type to protect the interconnections.

The W-type design offers a comparatively higher active area than the Z-type design as it avoids additional metallic interconnections.[104] Unlike the Z-type design, the neighbouring cells of alternative bias are interconnected in the W-type, as shown in Fig. 12d. Their simpler design and lack of additional serial interconnections can result in higher device FF values. The operation of W-type DSMs is different from that of Z-type ones because there are two types of cell configurations, *i.e.*, front illuminated (TiO_2 side, also called F-side) and back illuminated (Pt side, also called R-side) on the same module. The issue with W-type designs is their difficulty in matching the J_{SC} of these two different types.[98] The J_{SC} decreases in the R-side due to light absorption by iodide/triiodide and the low transmittance of platinum.[84] Thus, many optimisation procedures to match the J_{SC} of both types add complexity to the fabrication. However, SHARP Co. reported the highest confirmed η in W-type interconnected DSMs (8.2% and 9.3% with respect to active and total area, respectively); the active area (25.45 cm^2) was 85% of the total area.

One crucial requirement for both Z- and W-type designs is the separation required between neighbouring cells to avoid the mass transfer of electrolyte.[104] As the redox potential of the electrolyte changes when illuminated, a possible ion exchange between adjacent cells can separate the redox couple. This process is called photophoresis and is responsible for performance deterioration over time in DSMs. Thus, an individual cell must be a completely isolated compartment.

5.2.2 Parallel connection. Despite the high V_{OC} achieved by series interconnected DSMs, the required precision to match the J_{SC} of individual cells and the intensive care needed to interconnect the neighbouring cells to avoid lower FF and metal corrosion make their design and fabrication complex. On the other hand, parallel grid type DSMs offer ease of fabrication as they avoid the interconnection of working and counter electrodes (Fig. 12b). An example of such connections is the 'masterplate' designed by the joint research of various European institutions under the programme Nanomax.[128] In parallel connections, charge is collected not only from the bottom of the electrode in contact with the FTO, but also from the sides of the strips using metal grids (Ag, Ni, Cu Al, and Au).[49,110–114] These metal grids significantly enhance the photovoltaic performance of DSMs; a 100% increase in J_{SC}, a >200% increase in FF and a five-fold enhancement in η was reported for silver grids coated around large strips.[144] Späth *et al.*[94] reported the reproducible manufacturing of parallel connected DSMs (27 DSMs with a total area of ~100 cm^2) with $\eta \sim 4.3 \pm 0.07\%$. This method was further developed to deliver an η of ~7.4% employing silver in the current collecting grids.[115]

These designs can result in high FF; however, their major drawback is the low active area due to the silver current collectors, which need to be wide enough to collect the high currents with minimal voltage drops. Care must also be exercised to avoid the corrosion of silver grids by the iodide/triiodide electrolyte, for example, by using thick spacers (Surlyn or Bynel) to cover the grids.[57,104]

5.2.3 Ball grid DSC (BD-DSCs). Ball grid connection (based on ball grid array connection in electronic circuits) was introduced by NGK Spark Plug Co., Ltd., Japan to overcome lower FF when the electrode width was increased beyond a critical size.[43,116] This critical width is determined to be ~0.5–1 cm^2 such that the ohmic resistance of the film is reduced and a higher FF is offered.[102,117] The ball grid design (Fig. 13b and c) resembles monolithic designs as it employs only one substrate (FTO). These modules are connected in parallel and employ vertical metallic balls as current collectors; the major difference is that the electrons and holes are collected at the same side, unlike in other designs where electrons are collected from the FTO (Fig. 13c). The vertically oriented balls are connected to a flexible hybrid copper polyimide substrate and are taken to the external circuit. Surprisingly, the DSMs with areas of 8×8 cm^2 resulted in similar performances to that of a single cell (area ~ 0.5 cm^2); the DSMs showed an η of ~7–8% ($J_{SC} \sim 16$ mA cm^{-2}, $V_{OC} \sim 760$ mV, FF ~ 0.65) with a V_{OC} higher than that of a single cell. The remarkable performance of the ball grid, which also has commercial advantages, is due to its ability to retain the performance of a single cell during the scaling up process. It also has enhanced cost effectiveness as it eliminates the expensive Pt-coated CE. These designs do not require additional interconnections and external electrical connection; therefore, they result in very high active areas (95%), as shown in Fig. 13b.

5.2.4 Combined series and parallel connected DSMs. Until now, we have discussed various series or parallel connected DSMs that provide either added photovoltage or photocurrent, respectively. In these designs, one of the two parameters is compromised; the DSMs with high V_{OC} result in very low J_{SC} and *vice versa* (Table 3). To control the value of both of these parameters in a single device, which may be important for

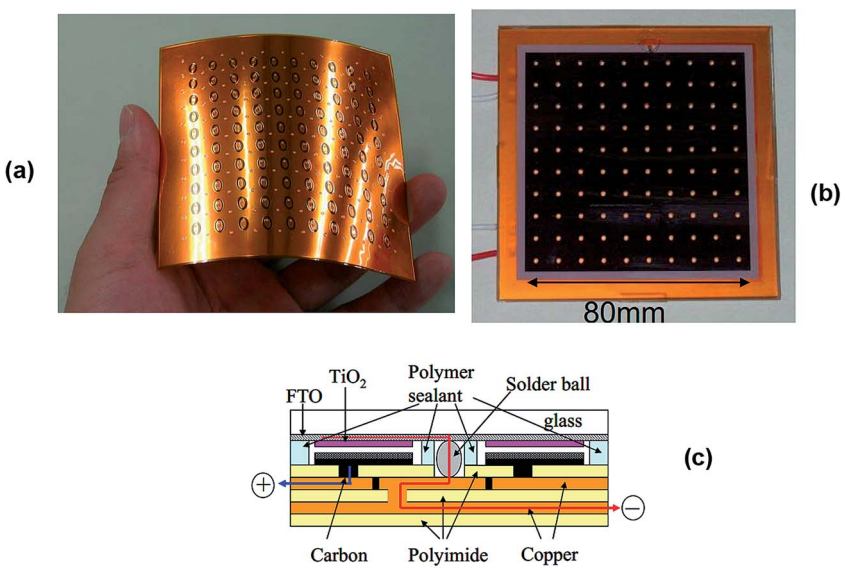

Fig. 13 (a) Solder shape ball connected on a flexible copper polyimide substrate, (b) an 80 mm square sub-module with η 7–8%, and (c) cross-section of a ball grid DSM. Figures are taken from an online report from NGK Spark Plug.

Table 3 A comparison of PV performance and device designs of a few DSMs. The percentages of active to total area are given to provide a meaningful comparison

Connection type	Active area (cm^2)	Active to total area	I_{SC} (mA)	V_{OC} (V)	FF	η (%)	Comments	References
Parallel (grid coated)	68	68%	NA	0.7	0.65	4.3	These designs are mostly grid coated using Ag or other metals such as Ni. This type of connection results in enhanced current density but creates stability issues in the device. To avoid exposure of the metallic grid to electrolyte, it should be encapsulated in sealant, adding complexity to the fabrication process.	94
	187	62.3%	1296	0.7	0.52	4.84		110
	81	81%	820	0.7	NA	4.3		111
	75	NA	50	0.76	0.7	5.7		49
	2246	63%	2100	9	0.62	5.9[a]		113
	18	73%	235	0.63	0.67	5.47[b]		114
	151	67%	2287	0.72	0.68	7.4[c]		115
	15.12	60.5%	172	0.75	0.66	5.52		97
	17.11 (ap. area)	NA	19.4	0.719	0.71	9.9[d]	The advantage of these designs is a more simple power management at the individual DSM level compared to series designs where high levels of current matching are required. These designs also survive reverse bias degradation	
Series + parallel	110	NA	120	2.2	NA	NA	This design reduces the active area available on the photoelectrode and provides lower J_{SC} but multiplies V_{OC}. The design is not widely adopted and has minimal potential for commercialization	103
	NA	NA	23.45	1.85	0.58	3[e]		144
	90	50	287	1.4	0.56	5.9		145
Z-type	43	73	51	9	0.65	7	Z-type DSMs provide good performance and high active area. However, they can suffer from lower FF due to excess interconnections that add to series resistance. Careful encapsulation of vertical connections is necessary	102
	47.5	47%	58	7.7	0.68	6.6		107
	505	74%	169	20	0.53	3.5		146
	512	73%	140	29	0.58	4.5		147
W-type	25.5	85%	54	6.3	0.61	8.2[f]	The highest certified efficiency reported in any DSM; however, careful design for current matching is required	84
Series monolithic	19.75	94%	28.55	3.9	0.61	5.29	Any mismatch of current in cells will affect the efficiency of the module. This design yields lower current density	60
	90.25	90.25%	40	9	~0.6	<2.5		106
Ball grid	80	95%	~1200	0.76	NA	~8%	Very high active area, similar performance to that of a single cell	116
DSCs (single cells)	~0.2		4.6	0.91	0.78	13	Routinely reported J_{SC} values in the best performing l-DSCs	26
	0.2	—	~4.6	0.93	0.74	12.3		148
	0.22	—	4.57	0.73	0.72	11.1		149
s-DSMs/quasi s-DSMs	100	~45%	37	5.16	0.47	0.8	Pore-filling, lower photoelectrode thickness, high stability	141
	625	46%	28	10.6	0.35	0.32		141
	112	52%	20	8	NA	0.9		142
	2.25	NA	20	0.62	0.50	2.8		150
	8	NA	~35	1.5	0.47	~2.5		86
	13.5	54%	21.5	3.2	0.39	2		87
s-DSCs	0.2	—	19.2	0.73	0.73	10.2[g]	The highest efficiency solid state laboratory scale device	151
Flexible DSMs	58	~60–70%	47	6.5	0.33	~3		124
	900	NA	77	6.7	<0.5	2–3%		101
	5.4	NA	69[h]	0.76	0.54	4.8	Devices fabricated on conducting plastic (PET/ITO) or metallic substrates such as titanium foil	123
	16.4	69%	30	3.8	0.53	3.3		46
	100	90%	727	0.72	0.73	6.7[i]		140
Large area panels	2246	63%	2100	9	0.62	5.9[a]	As per the definition of DSPs in Section 5.3, large area panels are ≥1000 cm^2	113
	14 000	74%	945[j]	4.5	0.56	3.58		100 and 143
	6000	48%	—	—	—	2.3		143

[a] At 0.84 sun, 64 series and parallel connected DSMs. [b] η 7% at 0.5 sun. [c] CE consisting of mixed Ti:Pt. [d] The value is taken from ref. 28, the original report stating the value was not found in our search. [e] 3D wire shaped DSM tree, *I–V* measured at 0.87 sun. [f] The highest certified η in DSMs. [g] Reported η is without a mask. [h] Calculated with respect to active area only. [i] Ti foil as a substrate and photovoltaic performance is reported at 55 mW cm^{-2}. [j] The reported photocurrent is only for a single DSM of area ~700 cm^2.

managing the electrical output of the module, combinations of series and parallel connection have also been attempted by researchers (Table 3).[148,149] Thus far, the best performing dually interconnected device resulted in an η of ~6% (V_{OC} ~ 1.4 V, I_{SC} ~ 287 mA, FF ~ 0.56) in a device of area ~90 cm^2. The issue here is very low active area; ~50% of the total area is utilized for

Table 4 Comparison of photovoltaic parameters of the three devices (S1–S3). The parameters are calculated by considering the active area (28 mm^2) and aperture area (28, 28.8, and 30.28 mm^2 for S1, S2 and S3 respectively). Reproduced from ref. 156

Device design	Dimensions & active area (cm^2)	I_{SC} (mA)	J_{SC} (mA cm^{-2})	V_{OC} (V)	FF	η_1 % (active area)	η_2 % (aperture area)
Single (S1)	~0.28	3.11	10.67	0.66	0.701	5.01	5.01
Split (S2)	$\sim 0.14 \times 2 = 0.28$	3.70	13.21	0.67	0.678	6.06	5.87
Split (S3)	$\sim 0.07 \times 4 = 0.28$	4.65	16.21	0.67	0.644	7.32	6.88

additional interconnections. Nevertheless, such designs are desired, especially when designing large area panels, as will be discussed in Section 8 (Table 4).

6. Fabrication of flexible modules

At present, the automated manufacturing of DSMs has steps (Fig. 10) that still require development for high volume and low-cost production. The rigid glass substrate used for DSM manufacturing, the high temperature required to evaporate the organic binders in the TiO_2 paste and electrolyte insertion are typical issues in the batch production of DSMs. Alternatively, various flexible substrates that are compatible with the roll-to-roll process can be introduced.[118–121] In addition to their flexibility, these substrates are also cost effective. For example, commercial plastic substrates (PET/ITO) available from Solaronix cost only one third of FTO-coated TCO.[122] However, additional encapsulation may be required, especially for long term outdoor operation, which can offset the lowering of cost. Flexible devices, however, are very desirable for applications where lightweight, conformable, flexible, thin power sources are sought. Furthermore, roll-to-roll high-throughput manufacturing can be applied.[19]

To utilize the flexibility of these substrates, various researchers have replaced the conventional FTO-coated TCOs with conducting plastic[123] and metallic substrates such as Ti foil or steel (Table 3).[124,125] For information on the developmental history of flexible DSCs and DSMs (f-DSMs), we recommend the comprehensive reviews by Weerasinghe *et al.*[126] and T. M. brown *et al.*[19] The first report on f-DSMs utilized a stainless steel substrate as WE and Pt-coated flexible plastic as CE, demonstrating an η of ~3% ($V_{OC} \sim 6.5$ V, $I_{SC} \sim 47$ mA, FF ~ 0.33).[124] The low observed FF for the less resistive metallic substrate is surprising and was attributed to high series resistance. However, a reference single cell also showed a similar FF and J_{SC} (~8 mA cm^{-2}); therefore, the low FF might be due to poor device fabrication and poor contact between the substrate and photoanode layer. This poor performance of a metallic substrate was later improved by Jen *et al.* by employing a Ti foil and growing ~35 μm vertically aligned nanotubes.[123] They employed a Pt-coated flexible polyethylene naphthalate (PEN)/ITO as CE. A parallel connected f-DSM (~5.5 cm^2) resulted in an η of ~4.8% ($V_{OC} \sim 0.76$ V, $J_{SC} \sim 13$ mA cm^{-2}, FF ~ 0.54). Here, a better contact between TiO_2 nanotubes and Ti foil resulted in a significantly improved performance; however, the stability of the devices has not yet been addressed. Conducting plastic substrates (PET/ITO and ITO/PEN) are widely employed as substrates in f-DSMs owing to their transparency. Ikegami *et al.*[101] reported an η of ~2% ($V_{OC} \sim 6.6$ V, $I_{SC} \sim 77$ mA, FF < 0.50) in DSMs (30 × 30 cm^2) on a PEN substrate. The corrosive electrolyte negatively affected the performance of these f-DSMs over time; their performance degraded ~40% after ~1000 h, primarily due to the removal of ITO from the substrate caused by reaction with electrolyte.

A mass production compatible process for the TiO_2 paste application remains elusive. Various methods employed so far such as anodization,[127–129] the lift up technique for a mesoporous highly conductive TiO_2 layer,[130] the compression method to enhance TiO_2 film interconnection,[131–135] and the printing of binder free paste *via* doctor blading[118,136] have hindered the roll-to-roll production of f-DSMs. Zardetto *et al.*[46] employed a UV irradiation process for the fabrication of both working and counter electrodes that is compatible with the roll-to-roll process and showed (i) $\eta \sim 4.3\%$ ($V_{OC} \sim 0.73$ V, $J_{SC} \sim 11$ mA cm^{-2}, FF ~ 0.56) in single cells and (ii) $\eta \sim 3.3\%$ ($V_{OC} \sim 3.8$ V, $J_{SC} \sim 1.8$ mA cm^{-2}, FF ~ 0.53) in W-contact modules with areas of ~17 cm^2. In another comparative study on the performance of flat and bent f-DSMs, the same group reported that bent DSMs can yield 10% extra power output compared to the flat device.[44]

The flexible DSMs routinely demonstrate lower FF and J_{SC} as a result of the high sheet resistance due to the poor contact between the mesoporous layer and the substrate along with the higher sheet resistance of the conducting substrates. The deposition of a thin TiO_2 layer *via* $TiCl_4$ solution treatment is a common practice in conventional DSCs to improve the adhesion of photoanode layers.[137–139] However, it cannot be applied on f-DSMs as it requires annealing at 450 °C before coating with the mesoporous TiO_2 layer. The flexible plastic substrates are not compatible with such a high temperature. Replacing conducting plastic with low resistivity metallic substrates such as steel did generate significant progress. Ti foil, however, is an often used material in this regard as TiO_2 nanostructures can be grown directly onto it with no adhesion issues between the substrate and the mesoporous layer. A study by Wu *et al.*[140] made a significant development towards this end, reporting an η of ~7% ($V_{OC} \sim 0.72$ V, $I_{SC} \sim 727$ mA, FF ~ 0.73) at 55 mW cm^{-2} in a flower-shaped mesoporous film directly grown on Ti foil. A high FF and J_{SC} (~8 mA cm^{-2}) were achieved due to the absence of additional interconnections, resulting in a high ratio of active to total area for the device (>90%). However, the η reported is at 55 W m^{-2}; therefore, the relationship between the performance

of f-DSMs with the high efficiency DSMs on TCOs is not straightforward.

7. Emergence of solid state DSMs

Although l-DSCs have achieved η >8% in DSMs and ~13% in DSCs, they are susceptible to performance degradation due to leakage and changes in redox species concentrations during the regeneration process.[81] Furthermore, electrolyte insertion is not a trivial process over large areas. Because of these issues, DSMs with alternative HTMs such as quasi-solid state electrolytes[141] and solid state hole conductors have been tested.[85] The s-DSMs using HTMs are relatively new and only a few reports have been published. The first report on s-DSMs employed poly-methyl-meta-acrylate (PMMA) and propylene carbonate to make a gel out of the conventional iodide/triiodide electrolyte.[141] Their series connected 100 cm^2 DSMs resulted in an η of ~0.8% (V_{OC} ~ 5.16 V, I_{SC} ~ 37 mA, FF ~ 0.47). They also demonstrated that s-DSMs can be fabricated without sealing the neighbouring cells; however, the performance of such DSMs dropped 60% in ~1000 h. Their upscaled s-DSMs with sizes up to ~625 cm^2 (23 serially connected DSCs with an active area of ~12.5 cm^2) showed relatively inferior performances compared to the DSMs with total areas of ~100 cm^2; the η dropped to 0.32%, mainly due to decreases in I_{SC} (28 mA) and FF (0.35). The lower FF and J_{SC} values (2–3 mA cm^{-2}) in both DSMs are primarily due to high series resistance (200–400 Ω) and reduced TiO_2 thickness (4–4.5 μm) compared to a conventional photoelectrode (15 μm), respectively. On the other hand, these modules showed a slight improvement in performance after 1000 h, unlike the liquid-based DSMs (l-DSMs). In a similar report, Freitas *et al.*[142] employed plasticized polymer electrolyte-based series connected s-DSMs (4.5 cm^2). Although a high V_{OC} ~ 8 V was obtained in outdoor testing, the low I_{SC} (~20 mA) resulted in a lower η <1%. Furthermore, the performance of these s-DSMs was rather discouraging after 1800 h; the devices retained only 30–40% of their original power output.

Unlike the l-DSMs, the performance of s-DSMs is significantly inferior compared to their single cells. In a comparative study by Snaith *et al.*,[86] serially connected 8 cm^2 s-DSMs employing mesoporous TiO_2/Al_2O_3 and spiro-OMeTAD showed an η of ~2% (V_{OC} ~ 1.5 V, I_{SC} ~ 35 mA, FF ~ 0.47), merely 25% that of a reference single cell with an area of ~0.12 cm^2. Low pore-filling (~40%) was found to be one of the factors contributing to low η in their modules, which can be improved by changing the solvent concentration of HTM and the porosity of the photoanode film. In a similar report by Matteocci *et al.*,[87] an η of ~2% (V_{OC} ~ 0.3.2 V, I_{SC} ~ 22 mA, FF ~ 0.39) was achieved on a TCO-based device on an active area of ~14 cm^2. The η was ~6.7% in flexible s-DSMs fabricated on Ti foil.[140] The researchers employed P3HT as the HTM with a TiO_2 nanoparticle photoanode.

The performances of s-DSMs are mainly hindered due to the poor infiltration of HTM into the mesoporous photoanode, unlike the liquid electrolyte, which easily penetrates throughout the TiO_2 film (~15 μm). Owing to the inferior pore filling (~40% in both reports where s-DSMS showed η >2%), the TiO_2 photoanode thickness is restricted to ~2 μm, resulting in a J_{SC} yield of only 30% compared to that of an l-DSM. The pore filling could be improved by using tubular or hollow nanostructures with high porosities (>60%) instead of nanoparticles, thus increasing the layer thickness to ≥10 μm. If these issues can be resolved along with the development of semi-transparency (*i.e.*, for BIPV) for these types of devices, s-DSMs will have strong industrial potential since they do not use volatile liquids, they have fewer lifetime issues, and their fabrication costs are expected to be cheaper than those of l-DSMs as they require less complicated sealing during fabrication.

8. Dye solar panels (DSPs)

For realistic commercial applications, DSMs must be transformed into larger panels for installation. The primary difference between DSMs and DSPs is their size, even though there is no clear description of size limit. In this article, we define a panel as having a photoelectrode size ≥1000 cm^2.

Numerous industrial developments in DSPs can be seen across the globe (Table 2); however, few experimental results regarding their performance have been published.[100,143] The first panel was reported in 2008 with a total area of >2 m^2; the individual modules had areas of ~300 cm^2 each.[113] The dually interconnected panel resulted in an η of ~6% on the active area (V_{OC} ~ 9 V, I_{SC} ~ 2.1 A, FF ~ 0.62) at 0.87 sun. This η is the highest reported for DSPs thus far. Subsequently, a joint European project termed 'ColorSol' was established to develop DSPs for BIPV applications;[100] DSPs of areas up to ~14 000 cm^2 (serially connected individual modules with areas of ~900 cm^2) resulted in η values of ~3.6% (V_{OC} ~ 4.55 V, I_{SC} ~ 945 mA, FF ~ 0.56) with respect to total area under 1 sun conditions (η = 4.6% with respect to its active area). These panels employed glass frit as the sealing material, resulting in high stabilities (~500 h). Both of these panels were manufactured by serially interconnecting individual DSMs; therefore, upscaling the DSC technology (*i.e.*, the development of an automated process for large scale panels) still remains a challenge. A study by Hinsch *et al.*[143] reported a semi-automatic process for the fabrication of DSPs up to ~1 m^2, which is an industrially viable size. Although the performances of these panels were lower (η <3%) than in previous reports, this is the first published report on the development of a semi-automatic reproducible process.

9. Summary of DSM development

All these designs have relative merits and drawbacks. Monolithic series are good in terms of continuous industrial mass production and cost effectiveness; however, they compromise on performance because of pore filling issues. Similarly, parallel (Ag grid encapsulated) designs are being developed by companies such as 3G solar, but they lead to problems for large areas as currents become so high as to cause problems in voltage drops. W-type is the simplest design to make, but has problems with current matching, which can limit efficiency and stability. Z-type delivers good performance, although their manufacture

is more complex due to the vertical interconnections and their encapsulation.

10. Emergence of alternative designs

10.1 Dye-solar module designs with improved FF

As described in Table 3, various designs of DSMs, s-DSMs, f-DSMs and DSPs have been fabricated to bring the device from laboratory scale to a level compatible with industrial mass production. These various types of connections resulted in devices with voltages as high as ~20 V and currents as high as ~2.5 A in separate devices. However, since the first report on large area DSCs, lower J_{SC} values have been routinely observed in DSMs compared to their single cell counterparts (Table 3). The highest confirmed J_{SC} in any DSM is ~18 mA cm^{-2}, as reported by L. Han *et al.*[84] in a W-type design and by Giordano *et al.*[102] in a Z-type design; however, routinely achieved J_{SC} values are much lower than that. The highest J_{SC} in any other design is ~15 mA cm^{-2} (in parallel designs). In contrast, the highest J_{SC} in a laboratory scale single cell is ~27 mA cm^{-2},[35] and J_{SC} >20 mA cm^{-2} is commonly obtained in high efficiency devices (Table 3).

This loss of 30–50% of the generated photoelectrons in large area devices is critical and is rarely explained in published reports. A few studies published on DSMs suggest that the comparatively lower J_{SC} in DSMs results from increased series resistance (R_S), which also affects the FF of these devices. This increased R_S originates from two sources: (i) the width of the TiO_2 photoanode; and (ii) the added metallic interconnections, particularly in series type DSMs.[100,117] The realization that TiO_2 width contributes to R_S was first experimentally demonstrated in 2006 by Biancardo *et al.*[141] The researchers varied the TiO_2 strip thickness from 2–0.5 cm and suggested that the lower thickness results in superior DSM performance; however, a clear trend between FF and R_S could not be drawn from their experimental results. In a subsequent report, Jun *et al.*[107] demonstrated the effect of photoelectrode dimensions (length and width of TiO_2) on FF. They first optimized the TiO_2 strip width (W_S) to be 0.8 cm for optimum FF (~0.65–0.62) by varying it from 0.25 to 3 cm. The FF dropped drastically from 0.65 to 0.3 when W_S increased from 0.8 cm to 3 cm. On the other hand, when the length (L) was varied from 5–15 cm at a W_S of ~0.8 cm, the FF showed no dependence on L. Similar dimensions are recommended by Zhang *et al.*[117] based on simulation and by Giordano *et al.*[98] based on experiments to design guidelines for DSM geometric parameters. The latter suggested that W_S be kept between 0.5 and 0.7 cm for photoelectrode lengths up to 15 cm as this provides the best compromise between aperture area and resistive loss. In another study using modelling of geometric dimensions, Giordano *et al.*[102] reported a systematic decrease in FF upon increasing W_S from 0.5–2 cm. Varying the L had no effect on the V_{OC} or J_{SC} of the devices. They correlated the R_{TCO} with the photoelectrode dimensions (W_S, L, and distance to the collecting electrode 'd') as:

$$R_{TCO} = R_{SHEET} \times \left(\frac{W_S + d}{L}\right) \quad (1)$$

Nevertheless, the optimization suggested in these reports only involves minimising the W_S to reduce the R_S offered by the substrate. In all the above reports, an increase in W_S is suggested as the primary source of the increase in R_S and thereby the drop in FF. However, even after minimising the width of the individual strips to <1 cm, the performance of DSMs is only <50–60% of that of DSCs at 1 sun.[152] Although it improved the FF of the DSMs, the suggested optimisation in these designs added a number of interconnections, reducing the aperture ratio of the modules. In addition, none of the reports on the optimisation of device geometry discussed the reasons behind the low J_{SC} in DSMs, and a comparative charge transport analysis of large area photoelectrodes with that of single cells is lacking. Therefore, a detailed understanding of charge dynamics is surprisingly still missing in the DSM literature.

10.2 Area dependent charge collection in DSMs

We note that all the adopted designs in DSMs are similar. In common practice, these modules are made in the form of large rectangular strips (Fig. 11a–c) with areas ≥3 cm^2 interconnected in either series, parallel or both. Many of these designs are adopted from other PV technologies; the parallel or grid connections are adopted from amorphous silicon solar cells, while the series interconnections are inspired by thin film modules. Recent studies by Fakharuddin *et al.*[153–157] suggest that these designs do not work well for DSMs due to their diffusive charge transport in a "soft" environment, which is largely different from the first two generation solar cells. Notably, due to the neglect of charge transport parameters while upscaling the DSCs, significant current collection comes only from a limited region of the photoelectrode. For example, under similar experimental conditions, ECN researchers obtained $\eta \sim$ 12% in their single cells and $\eta \sim$ 4–5% in ~225 cm^2 modules in a masterplate design.[105] Such trends are routinely seen in DSMs; their J_{SC} (Table 3) values are significantly smaller than those of DSCs.

It is important to note that charge transport in DSCs occurs *via* hopping or trap-mediated conduction through n-MOS, which are several orders of magnitude slower than transport through single crystalline semiconductors.[158–163] Due to diffusive charge transport and the competitive situation where the generated electrons are rapidly intercepted by the electrolyte ions, the photoelectrode thickness is limited to below ~15 μm in single cells (area ≤ 0.2 cm^2). Currently, diffusion length ($L_n = (D_n\tau_n)^{1/2}$) is the only defined parameter considered for the complete collection of photogenerated electrons in TiO_2 films,[164–166] where D_n is the electron diffusion coefficient and τ_n is the electron lifetime (*i.e.*, the length above which electrons recombine with holes in the electrolyte). In recent experiments, the number of paths and path lengths of electron diffusion have been observed to increase during scaling up; therefore, the device parameter L_n has limitations in DSMs.[156,157] We first reported that η drops bi-exponentially upon increasing the active area in the photoelectrode for TiO_2 NPs.[154] The η drops off three-fold when the photoelectrode area is increased in the range of 0.15–2 cm^2; the main contributor to this drop is the

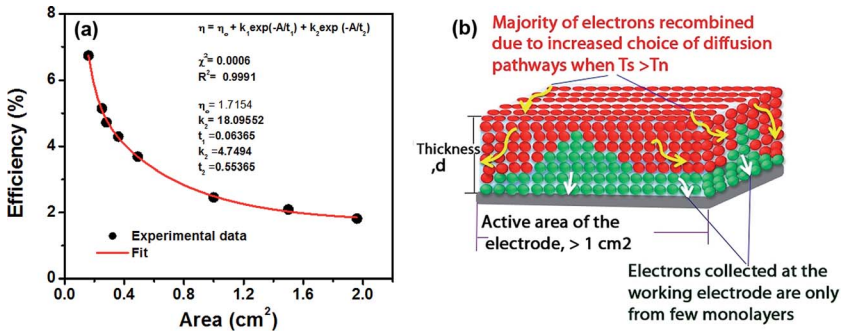

Fig. 14 (a) The efficiency of a DSC decreases bi-exponentially with increasing device area in a range of 0.15 cm^2–2 cm^2 and (b) schematic showing electron collection from only a fraction of the photoelectrode film nearer to the WE in DSCs with large photoelectrode areas. Figure reproduced from ref. 153.

drop in J_{SC} (Fig. 14a). The detailed charge transport studies of these devices suggest that upon increasing the photoelectrode area, the recombination resistance (R_{CT}) decreases and the electron transport time (τ_d) increases; consequently, only the photoelectrons from a fraction of TiO_2 (few microns) nearer to the working electrode are collected (Fig. 14b). A similar concept was reported by Halme *et al.*,[22] who suggested based on device simulations that the possibility of electrons being collected is higher if they are produced nearer to the working electrode substrate. As the τ_n is several tens of milliseconds in DSCs employing TiO_2 NPs, a high R_{CT} and low τ_d (10–100 times smaller than τ_n) is preferred for high efficiency devices.[20,167]

These studies show that the L_n alone as a device parameter has limitations in the description of photoelectron collection in large area DSCs; a three-dimensional analogue such as diffusion volume (V_n) is suggested as a possible alternative. In the experiment designed in ref. 157, which employs three photoelectrodes of similar active volumes but different device designs (Fig. 15a), restricting the diffusion pathways in three dimensions by appropriate device designs resulted in enhanced J_{SC} and η in photoelectrodes of similar active volumes (Fig. 15b). Upon increasing the photoelectrode area, the competition between τ_n and τ_d becomes crucial. Given a τ_n of a few milliseconds, the photoelectrons beyond a limit are never collected due to their longer τ_d. A ~20% greater charge collection efficiency (η_{cc}) in those designs was demonstrated by considering V_n, resulting in an overall enhancement in η; $\eta = f(\alpha, \phi_{in}, \phi_{reg}, \eta_{cc})$. The α (absorption coefficient), ϕ_{in} (injection efficiency) and ϕ_{reg} (dye-regeneration efficiency) are the same in all the devices as they are made of similar materials and have similar photoelectrode thicknesses (~14 μm) (Fig. 15).

Based on our insights into photoanode area dependent DSC performance, we tested various module designs with unit cells of 1–100 mm^2 as shown in Figure 16(a–c). We note that such split designs likely add difficulty in the fabrication process as the sealing and interconnection of individual cells will become a major issue. However, such designs have a greater probability of success in s-DSMs as the concentration differences in redox species between neighbouring cells do not arise in solid electrolytes. Based on the connection types, these cells are likely to provide very high photocurrents or photovoltages in DSMs.

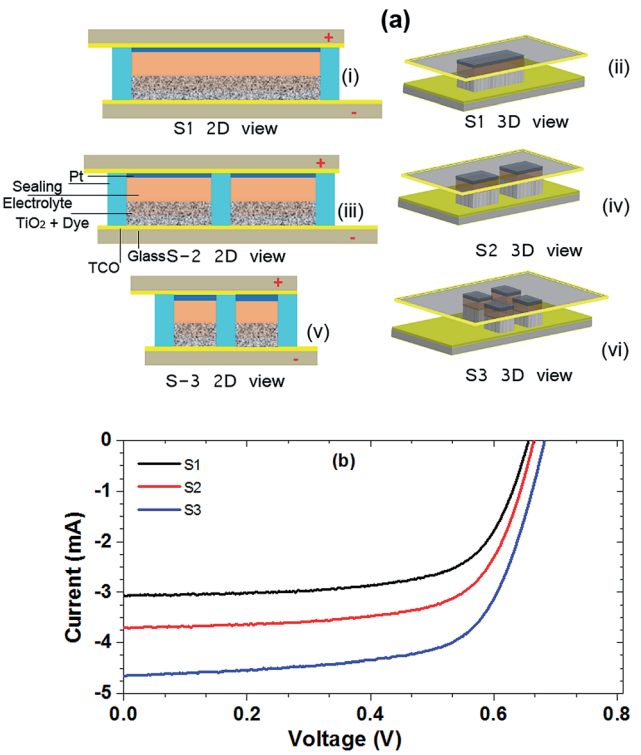

Fig. 15 (a) Schematic of stacked cells on a single substrate and (b) *I*–*V* curve of the three DSCs. Figures adapted from ref. 157.

An alternative to avoid lateral diffusion and improve the η_{cc} could be the use of vertically aligned one-dimensional structures such as nanowires or nanotubes that would keep constant values of J_{SC} even with increased electrode area. Unfortunately, to date, the use of these kinds of nanostructures in small area DSCs has not resulted in comparable J_{SC} values with respect to nanocolloidal films due to their lower roughness and thus dye uploads.

11. DSM stability tests

For DSC technology to be commercially successful, their long term performance under device working conditions such as

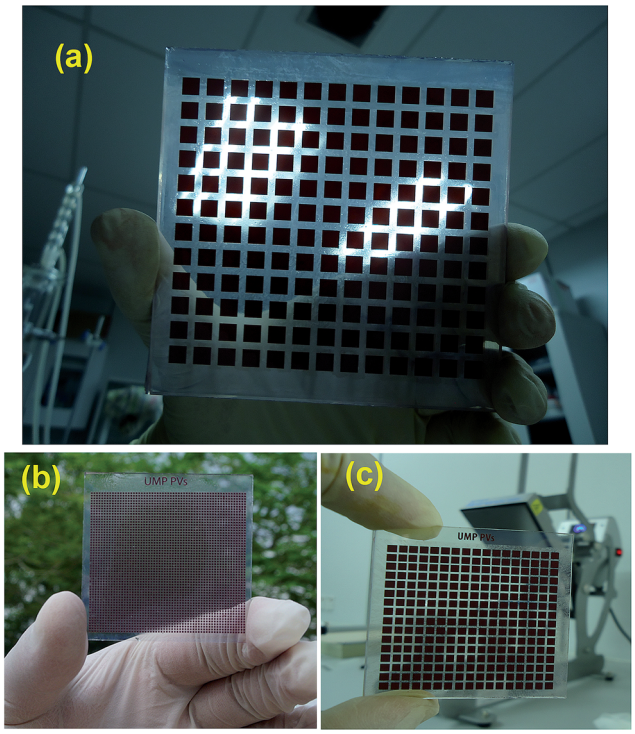

Fig. 16 (a) A DSM photoelectrode (100 cm^2) printed at the Nanostructured Renewable Energy Materials Laboratory, Faculty of Industrial Sciences & Technology, Universiti Malaysia Pahang laboratory with individual cell dimensions of 0.5 cm × 0.5 cm with 2 mm interspacing, (b) a 25 cm^2 printed electrode with tiny dots of 1 mm^2 and interspacing of ~0.3 mm, and (c) a 25 cm^2 photoelectrode with individual cell sizes of 4 mm^2 and an interspacing of ~1 mm. Such designs are expected to yield very high J_{SC} or V_{OC} depending on the type of interconnection.

high temperature, humidity, and continuous light illumination must be ensured. The commercial deployment of DSCs requires device working performance without significant degradation for >10 years,[168] especially when their competitors (*i.e.*, silicon PVs) perform for ~25 years while retaining >80% of the original η. Here, we separately discuss the stability of (i) various components of DSCs such as dyes and electrolytes and (ii) the long term outdoor stability of DSMs.

11.1 Thermal stability of dyes and electrolytes

The organic materials of DSCs are known to suffer high degradation rates when exposed to ambient conditions.[169] In addition, liquid electrolytes cause leaking and corrode the metallic grids used for interconnections if not properly encapsulated. In DSCs, the stability is primarily associated with the hermetic sealing; the sealants should be stable at high temperature and passive to liquid electrolytes, and in case of spot sealing failure (pinholes), the materials chosen for grids should be corrosion resistant, and the design should be robust enough to avoid spreading of the electrolyte out of the cell compartment.

The ECN started the Joule program (LOTS-DSC JOR3-CT98-0261) to realise device outdoor performance capabilities over ~10 years.[170,171] They investigated DSC stability under intensive light (2.5 sun) as well as thermal stability at temperatures up to 80 °C. Their masterplate design using a Surlyn spacer with η ~ 5–6% showed stability up to 8300 h at 2.5 sun, a time equivalent to ~10 years of outdoor operation. The η decreased <10% for 2000 h operation at 60 °C; at 80 °C, the decrease was 30%.[49] Such thermal stability is achieved by chemically changing the iodide/triiodide based electrolyte composition *via* the addition of MgI_2 and CaI_2. The higher temperature induces instability to (i) the dye molecules by detaching them from the TiO_2 surface,[172] and (ii) the electrolyte components such as *tert*-butyl pyridine(TBP) and lithium iodide (LiI) during thermal aging.[49] To improve the high temperature stability of dyes, co-grafting it with 1-decylphosphnic acid (1-DPA) or hexadecylmalonic acid (HDMA) is suggested as a possible solution.[173,174] Although the above procedure improved the integrity of the dye–TiO_2 surface, the additional dilution reduced the amount of dye-anchoring and light harvesting. A major advancement in electrolyte stability was reported by Grätzel *et al.*,[172] who introduced a low volatility robust electrolyte in conjunction with an amphiphilic ruthenium sensitizer (K19). In their study, ~8.2% efficient DSCs retained 98% of their original performance after soaking for 1000 h at 60 °C in light. The thermal stability of the above dye–TiO_2 conjugate was further verified at 80 °C in the dark. Through these studies, the DSCs achieved the specifications laid out for the outdoor performance of silicon solar cells for the first time.

A significant advancement in DSC performance at temperatures >80 °C was reported by Dyesol Ltd. By employing stable dyes (N709 and Y123) and a 3-methoxypropionitrile (MPN)-based electrolyte, the DSCs showed stabilities of over 90% for 1000 h at 95 °C.[91] The major contributor to the observed ~10% drop in η came from the V_{OC} originating from the change in redox species concentration in the electrolyte. Other photovoltaic parameters (J_{SC} and FF) showed no notable degradation. These results are encouraging and suggest that DSC technology can possibly be deployed in extremely hot places.

The substitution of Surylin with other more stable sealants such bynel (EPFL), frits (ECN) or UV-cured epoxy composite sealants (Dyesol) has been a key factor in these advancements. Surylin starts softening at 70 °C, making it unsuitable for high temperature applications, and is permeable to water, which may cause long term stability problems.

11.2 Long term stability of DSMs

Only a few studies to date have reported on DSM stability. In general, DSM stability is inferior to those of their laboratory counterparts. In 2004, a research group of AISIN SEIKI carried out the first outdoor stability testing of DSMs (64 serially connected cells of 10 × 10 cm^2) for over half of a year.[108] Surprisingly, no significant effect of moisture on device performance was noticed. They reported that a DSM generated comparatively more electricity than a silicon-based cell over one year due to: (i) the superior performance of DSMs in low light; (ii) the improved rheology of the electrolyte at higher temperatures; and (iii) their weaker dependence on the angle of light incidence. The devices showed an ~20% drop in output power after one year of operation, although the source of this drop was not elaborated upon

with the exception of the reported electrolyte leakage in a few cells. This drop in output power was overcome in an extended investigation using a set of experimental techniques to determine the contribution from each DSM component to its performance degradation.[103] This study showed remarkable long term (2.5 years) outdoor stability results: (i) no electrolyte leakage was found in the device; and (ii) the dye (N719) and carbon counter electrode were stable, as confirmed by Raman spectroscopy and the stable J_{SC}. However, the concentration of triiodide is still reduced in the electrolyte. This effect was attributed to irreversible reactions between iodide and iodine species with water present in the electrolyte, leading to electrolyte bleaching and the irreversible formation of:[175,176]

$$\begin{aligned} &3I_3^- + 6OH^- \leftrightarrow IO_3^- + 3H_2O + 8I^- \\ &I^- + 6OH^- + 6h^+ \leftrightarrow IO_3^- + 3H_2O \\ &3I_2 + 3H_2O \leftrightarrow IO_3^- + 6H^+ + 5I^- \end{aligned} \quad (2)$$

These reactions have been shown to be enhanced by UV light and temperature.[176,177] Electrolyte bleaching is also dependent on the electrolyte solvent and its origin, which are not yet clearly stated, associated with TiO_2–electrolyte or TiO_2–dye–electrolyte interactions.[178] Good sealing and low humidity conditions during the fabrication process are then required to obtain good long term stability results.

Towards the thermal stability testing of DSMs, a report by Kroon *et al.*[179] of ECN showed significantly stable (80%) performance at >80 °C for 3000 h. The devices showed a decrease in power output of ~20% using a robust electrolyte. In another study by Mastroianni *et al.*,[99] the stability of DSMs (30 cells with an area of 3.6 cm^2) were tested in indoor (at AM 1.5 G and 85 °C) and outdoor (horizontally placed and tiled at 25°) conditions. For a period of 3200 h, the outdoor DSMs were significantly stable, with only a 10% decrease in their original efficiency. However, the vertically placed outdoor cells showed greater degradation at maximum power point due to the uneven triiodide concentration, indicating that the vertical orientation of l-DSMs affect device lifetime. A detailed impedance characterization also revealed a reduction in the diffusion length and a possible alteration at the TiO_2/electrolyte interface.

Asghar *et al.*[169] summarized the major instability issues in a recent review and suggested that (i) Z709 and K19 are the only stable dyes at a temperature of ~80 °C, and (ii) devices mostly employing polymer and ionic liquid electrolytes passed light soaking tests (60 °C) and thermal stress tests (80 °C) for 1000 h. Although significant advancements have been made towards determining the stabilities of DSCs and DSMs, such reports were limited to glass substrate-based devices. The stabilities of flexible DSCs/DSMs at temperatures >50 °C are yet to be investigated, although such devices have shown considerable stabilities up to 50 °C.[180] Furthermore, a standard criterion is needed for the investigation of stability because devices undergo chemical changes when exposed to outdoor conditions; therefore, chemical investigations along with electrical characterisations are essential when reporting stability analyses.

DSM design involves more complexity compared to the simpler DSCs, and the sealing process is consequently more difficult. To avoid failure in a single point of the sealing that ruins the performance of a complete module, it is necessary that the external components that may be affected by direct contact with leaking electrolyte do not degrade. Of particular importance are the collecting grids; silver should be avoided in the most exposed sections of the cells as iodide reacts very efficiently with it. Alternative materials for collecting electrodes may be carbon, titanium or tin (at the cathode).

Robust module designs must consider ways to control or neutralize the occurrence of localised electrolyte escape. The use of gellified electrolytes,[181,182] solid electrolytes or double sealing structures (Fujikura) may help to avoid the loss of electrolyte and thus improve module performance.

11.3 Reverse bias degradation of DSMs

With respect to single cells, the stability of modules is considerably more complex due to the fact that large areas increase the probability of disuniformities and defects, which can lead to increased degradation rates or failures (*e.g.*, non-uniform coverage or pinholes in the encapsulation or interconnections). Furthermore, when cells are connected together in series in a module, the possibility of the occurrence of reverse bias degradation effects must be considered. In fact, a cell that is electrically mismatched in a module, which occurs when it is shadowed or has degraded at a higher rate compared to other cells, can become inversely polarized by the other well-performing cells in the system.[146] Current is then forced though it by the other cells. Over the long term, this can lead to device degradation and even failure.[183] Contributing to reverse bias degradation are triiodide depletion and the presence of impurities, particularly water. Developing a further understanding of reverse bias phenomena acting upon these components and setting up diode protection strategies is important for delivering long-lasting DSMs.[184]

12. Standards for DSMs

With some exceptions, due to the relative infancy of industrial development, reports on systematic statistical long term outdoor testing are scarce. At the moment, stability testing on DSMs involves protocols developed for thin films. Even though more statistics and continued tests are required, some promising developments have been reported. DSMs have passed thermal stability testing (IEC 1215), although with η values decreased by 30–40%. Fujikura have shown that cells and submodules have passed several endurance tests according to JIS C 8938 standards.[185] Dyepower has reported successful UV preconditioning, humidity freeze and damp heat IEC 61646 tests carried out over large area (>500 cm^2) DSC modules.[186] The IEC tests are meant only for indoor analysis and do not consider the chemical changes that DSMs undergo upon exposure to atmospheric conditions. For DSMs, a different set of standards are required that analyse device performance in conditions close to natural outdoor conditions and account for chemical changes such as UV-stability and chemical stability under atmospheric conditions.

For DSMs to be a successful commercial product, they must pass few standards that are widely applied to silicon and thin film solar cells such as IEC 61646, IEC 1215, IEC 1646, and IEC 1215. These standards are necessary to ensure sufficient device stability over the required lifetime. Test protocols tailored for DSC technology have yet to be designed and implemented. Additionally, there is also a need to set standards for DSM fabrication and characterisation because different fabrication techniques and experimental conditions result in significant variation in η (Sections 5–9). A similar standardisation has been suggested by Yang *et al.*[187] for the reliable evaluation of laboratory scale DSCs involving the calibration of the solar simulator *via* reference cells, the measurement time of the photovoltaic characterisations (*I–V* & incident photon-to-current conversion efficiency), and the masking process. Nevertheless, absence of such standards for DSMs leads to misconceptions, particularly in the reporting of module efficiency values; a number of researchers reported η with respect to active area, while others reported with respect to active and aperture area. Ultimately, the latter is the most important number. In fact, since aperture ratios (the ratio between active and aperture areas) can differ greatly depending on the construction methods, the performance on active area and aperture area of DSMs can differ significantly. In the literature, aperture ratios vary from 85% (ref. 84) to less than 50%;[141] thus, η drops between 85% and less than half of the reported active area value when total area is considered. It is important that both numbers are given.

13. Conclusions and future projections

Any PV technology entering the market has usually been pitched in terms of three main parameters: (a) efficiency, (b) lifetime and (c) cost. Over 80% of the current market is cornered by silicon cells, which remain the benchmark for PV systems. Over the last few years, the price of silicon modules has decreased considerably. In fact, the drop has been so significant that in 2012, the average cost of modules dropped below the significant threshold of 1$/Wp (*i.e.* ~0.8$/Wp).[188] While part of this is due to oversupply in the market, a significant portion is due to advances in technology and economies of scale resulting from an increase in cumulative worldwide PV production. Thus, whereas a decade ago new technologies may have aimed at also competing on cost calculated in $/Wp, a more suitable roadmap today considers the development of applications where the new technology offers competitive advantages in functionality over silicon or other existing PV technologies. In Fig. 17, we have added a technological "functionality" entry to the competitive mix in which DSM must compete.

Fig. 17 helps identify entry or niche market products (each with a different mix of the three parameters and associated technological functionalities) on which particular DSM technology development can be focused. Subsequently, the market space will grow with continued R&D development, and economies of scale will kick in so that in the longer term, the technology may even enter the more conventional PV system arena. The capital cost to implement industrial fabrication of DSMs is another advantage of this technology as the required investments are one order of magnitude smaller compared to standard technologies. The roadmap for the technological development of DSMs depends strongly on the application. This also explains why different DSM designs and architectures are being explored (*e.g.*, glass, flexible, liquid-based, solid state, monolithic, double plate Z, W or parallel, *etc.*).

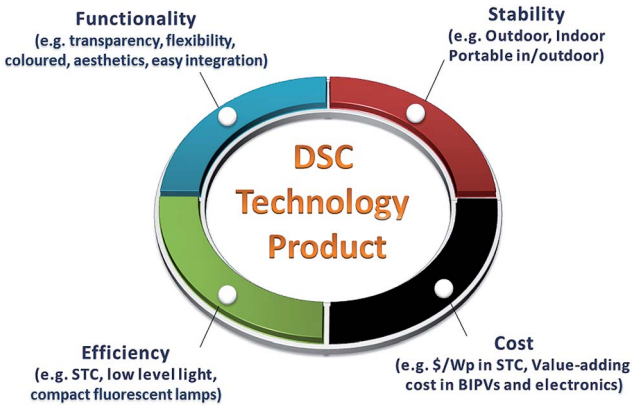

Fig. 17 Scheme representing inter-relations between the three parameters (power conversion efficiency, stability and cost) that must be considered together with functionality for the successful industrial product development of dye-solar cell modules. Different applications and markets lead to different mixes of requirements and thus different DSM technological developments (*e.g.*, glass, flexible, material combinations, device architectures, *etc.*).

Although there are many commercial developers of materials and technology working on various aspects of DSMs and prototypes, the market where available commercial products integrate DSMs (at the time of writing) is represented by electronic products, especially those for portable or indoor uses.[19] G24 Power Ltd. provides DSMs for these applications that are made with flexible titanium foil working electrodes and plastic/ITO counter electrodes and are series connected.

Due to their remarkable performance under low levels of light and compact fluorescent lamps, there is strong interest in both glass-based products (http://ricoh.com/release/2014/0611_1.html) and even more so in thin flexible DSMs (http://www.gcell.com), which can be easily integrated in fixed or portable electronic products such as sensors in the home and personal computer peripherals. Although the efficiencies of these flexible modules are still not particularly high under STC, their power output has been shown to outperform competing technologies including amorphous silicon (the current most suitable technology) under indoor lighting.[18] The commercialisation of these products with integrated DSMs has been enabled by the fact that their efficiencies are particularly high indoors, their flexibility and light weight characteristics permit easy integration (and portability), their degradation rates are reduced in less-harsh indoor conditions and their lifetimes of a few years (similar to that of the electronic product they are integrated on) are commercially acceptable. Thus, in this

particular arena, the DSMs deliver functionalities that conventional crystalline silicon does not. The cost here is not measured in $/Wp, but in the added value that their integration brings (*e.g.*, eliminating the need to replace batteries). The developmental roadmap for flexible devices involves continuing to diminish costs (opening up the possibility of integrating the devices in cheaper products) and increasing lifetimes, particularly outdoors (for portable or semi-fixed/portable installations), by researching better performing (and cheaper) material combinations and encapsulation barrier strategies. Furthermore, the development of efficient hole blocking compact layers at the working electrode is particularly important under low levels of illumination.

A huge market for DSMs is represented by BIPVs, where devices can be incorporated into big installations worth hundreds of millions of dollars globally. Development work by various industrial entities (see Table 2) is on-going to produce prototypes and demonstrators for integration in applications such as bus shelters, roofing and building facades, including semi-transparent windows.[189] The latter is particularly suited for DSMs because most technological development has been carried out on glass. Glass also has exceptional barrier properties (which is crucial for lifetimes) and is becoming an ever more widespread material for modern buildings. For integration in shelters, lifetimes of a few years can suffice; however, integration in buildings requires very challenging lifetimes exceeding 15–20 years. Glass DSM technology brings the competitive advantage of enabling the power-generating unit to be semitransparent.[190] In fact, the transparency *versus* efficiency of the DSM can be tuned depending on the requirements for energy generation, visible light transmission and colour.[17] For properly rating glass facade applications, the efficiency parameter at STC should be at least complemented by other parameters such as energy produced over the course of the year in real environmental conditions,[191] which depends strongly on location, both geographic and related to the building (*e.g.*, vertical or tilted conditions). DSMs have been shown to deliver 10–20% more energy (at the same power rating) compared to silicon installations (even though efficiencies still remain significantly lower).[108] For BIPV applications, perfecting encapsulation and developing more stable dyes, less volatile electrolytes with stabilizing additives, and quasi or fully solid-state carrier mediators are paths used by researchers to improve stability. For large scale installations, the uniformity and tolerances that can be achieved in the manufacturing process over (very) large areas together with the management of the electrical output power of the modules (and panels) are important and complex issues to be tackled. The most suitable device architecture can depend on the size of the unit module that makes up the panel. Parallel, series or combined interconnections can be selected to deliver the required voltage and current levels. Electrical and diode protection strategies will also differ depending on the type and size of the module. For BIPVs, as much as the $/Wp, it is important to consider the marginal added costs with respect to conventional building materials (*e.g.*, the cost of a façade with PV functionality compared to that without). Much of the engineering work needed to bring efficiency, stability and costs to the levels required by the BIPV industry along with the peculiar functionality of DSMs required by the markets is being carried out, often "quietly" in industrial R&D divisions, and results and developments are only partly publicly available. The growing activity in patent filing in this field shows (see Fig. 6a), however, that intense work is being carried out to bring the technology to market, and, at the same time, that there are tremendous opportunities for exciting innovation in the field.

While a great body of research is carried out on improving laboratory scale DSCs, little attention is paid to their large area devices; research on DSMs is ~1% of that on DSCs. Due to this negligence, the η of DSMs has shown comparatively little improvement since their first report (5.6% in 1996). The maximum η reported for DSMs is 8.2% through optimized front and back illumination, which is still significantly lower than that obtained in high efficiency single cells (~13%). The lack of focus towards device engineering and a complete negligence of charge transport in DSMs are the main factors behind the comparatively lower performance of DSMs.

Acknowledgements

This work was financially supported by the ministry of higher education of Malaysia through a prototype research grant scheme. We also acknowledge support by a project from Generalitat Valenciana (ISIC/2012/008). We are thankful to David Martineau of Solaronix Ltd. and Damion Milliken of Dyesol Ltd. for sharing information on the comparative performance of DSMs, and also to Iván Mora Seró for discussion on DSC cost analysis. The authors also thank Dr Hans Desilvestro of Dyesol for useful discussion on the 'route to DSMs' future'.

References

1 Key World Energy Statistics, http://www.iea.org/publications/freepublications/publication/KeyWorld2013.pdf, accessed December 2013.
2 M. Grätzel, *Acc. Chem. Res.*, 2009, **42**, 1788–1798.
3 R. Perez, K. Zweibel and T. E. Hoff, *Energy Policy*, 2011, **39**, 7290–7297.
4 J. Nelson and C. J. Emmott, *Philos. Trans. R. Soc., A*, 2013, **371**, 4.
5 P. Docampo, S. Guldin, T. Leijtens, N. K. Noel, U. Steiner and H. J. Snaith, *Adv. Mater.*, 2014, **26**, 4013–4030.
6 Solar generation PV capacity, http://www.bp.com/en/global/corporate/about-bp/statistical-review-of-world-energy-2013/review-by-energy-type/renewable-energy/solar-energy.html, accessed January 2014.
7 H. Wirth, http://www.ise.fraunhofer.de/en/publications/veroeffentlichungen-pdf-dateien-en/studien-und-konzeptpapiere/recent-facts-about-photovoltaics-in-germany.pdf, accessed November 2013.
8 ZSW press release, http://www.zsw-bw.de/uploads/media/pi18-2013-ZSW-WorldrecordCIGS.pdf, accessed December 2013.
9 NREL: Best research cell efficiencies, http://www.nrel.gov/ncpv/images/efficiency_chart.jpg, accessed May 2014.

10 First Solar, http://www.firstsolar.com/Innovation/Advanced-Thin-Film-Modules, accessed December 2013.
11 B. E. Hardin, H. J. Snaith and M. D. McGehee, *Nat. Photonics*, 2012, **6**, 162–169.
12 British Petroleum review, bp.com/statisticalreview, accessed November 2013.
13 IEA, http://www.worldenergyoutlook.org/media/weowebsite/2012/PresentationtoPress. pdf, accessed January 2014.
14 M. Grätzel, *J. Photochem. Photobiol., C*, 2003, **4**, 145–153.
15 A. Hagfeldt, G. Boschloo, L. Sun, L. Kloo and H. Pettersson, *Chem. Rev.*, 2010, **110**, 6595–6663.
16 J. Bisquert, *ChemPhysChem*, 2011, **12**, 1633–1636.
17 R. Tagliaferro, D. Colonna, T. M. Brown, A. Reale and A. Di Carlo, *Opt. Express*, 2013, **21**, 3235–3242.
18 N. Sridhar and D. Freeman, *Proceedings of 26th European Photovoltaic Solar Energy Conference and Exhibition*, hamburg, Germany, 2011.
19 T. M. Brown, F. De Rossi, F. Di Giacomo, G. Mincuzzi, V. Zardetto, A. Reale and A. Di Carlo, *J. Mater. Chem. A*, 2014, **2**, 10788–10817.
20 Q. Wang, S. Ito, M. Grätzel, F. Fabregat-Santiago, I. Mora-Seró, J. Bisquert, T. Bessho and H. Imai, *J. Phys. Chem. B*, 2006, **110**, 25210–25221.
21 J. Bisquert, *Phys. Chem. Chem. Phys.*, 2008, **10**, 49–72.
22 J. Halme, P. Vahermaa, K. Miettunen and P. Lund, *Adv. Mater.*, 2010, **22**, E210–E234.
23 G. Boschloo and A. Hagfeldt, *Acc. Chem. Res.*, 2009, **42**, 1819–1826.
24 T. Daeneke, T. H. Kwon, A. B. Holmes, N. W. Duffy, U. Bach and L. Spiccia, *Nat. Chem.*, 2011, **3**, 211–215.
25 Y. Liu, J. R. Jennings, Y. Huang, Q. Wang, S. M. Zakeeruddin and M. Grätzel, *J. Phys. Chem. C*, 2011, **115**, 18847–18855.
26 S. Mathew, A. Yella, P. Gao, R. Humphry-Baker, B. F. E. Curchod, N. Ashari-Astani, I. Tavernelli, U. Rothlisberger, M. K. Nazeeruddin and M. Grätzel, *Nat. Chem.*, 2014, **6**, 242–247.
27 T. Yamaguchi, N. Tobe, D. Matsumoto, T. Nagai and H. Arakawa, *Sol. Energy Mater. Sol. Cells*, 2010, **94**, 812–816.
28 M. A. Green, K. Emery, Y. Hishikawa, W. Warta and E. D. Dunlop, *Prog. Photovoltaics*, 2014, **22**, 1–9.
29 R. Harikisun and H. Desilvestro, *Sol. Energy*, 2011, **85**, 1179–1188.
30 D. Bari, N. Wrachien, R. Tagliaferro, T. M. Brown, A. Reale, A. Di Carlo, G. Meneghesso and A. Cester, *Microelectron. Reliab.*, 2013, **53**, 1804–1808.
31 D. Xiong and W. Chen, *Front. Optoelectron.*, 2012, **5**, 371–389.
32 J. H. Im, C. R. Lee, J. W. Lee, S. W. Park and N. G. Park, *Nanoscale*, 2011, **3**, 4088–4093.
33 I. E. Castelli, T. Olsen, S. Datta, D. D. Landis, S. Dahl, K. S. Thygesen and K. W. Jacobsen, *Energy Environ. Sci.*, 2012, **5**, 5814–5819.
34 M. J. Carnie, C. Charbonneau, M. L. Davies, J. Troughton, T. M. Watson, K. Wojciechowski, H. Snaith and D. A. Worsley, *Chem. Commun.*, 2013, **49**, 7893–7895.
35 H. S. Kim, J. W. Lee, N. Yantara, P. P. Boix, S. A. Kulkarni, S. Mhaisalkar, M. Grätzel and N. G. Park, *Nano Lett.*, 2013, **13**, 2412–2417.
36 N. G. Park, *J. Phys. Chem. Lett.*, 2013, **4**, 2423–2429.
37 J. You, Z. Hong, Y. Yang, Q. Chen, M. Cai, T.-B. Song, C.-C. Chen, S. Lu, Y. Liu and H. Zhou, *ACS Nano*, 2014, **8**, 1674–1680.
38 F. Hao, C. C. Stoumpos, D. H. Cao, R. P. H. Chang and M. G. Kanatzidis, *Nat. Photonics*, 2014, **8**, 489–494.
39 F. Matteocci, S. Razza, F. Di Giacomo, S. Casaluci, G. Mincuzzi, T. M. Brown, A. D'Epifanio, S. Licoccia and A. Di Carlo, *Phys. Chem. Chem. Phys.*, 2014, **16**, 3918–3923.
40 J. Seo, S. Park, Y. Chan Kim, N. J. Jeon, J. H. Noh, S. C. Yoon and S. I. Seok, *Energy Environ. Sci.*, 2014, **7**, 2642–2646.
41 S. Ubertini and U. Desideri, *Renewable Energy*, 2003, **28**, 1833–1850.
42 Dyesol, http://www.dyesol.com/about-dsc/advantages-of-dsc, accessed 13 December 2013, 2013.
43 K. Kalyanasundaram, *Dye-sensitized Solar Cells*, CRC press, Switzerland, 1st edn, 2010.
44 V. Zardetto, G. Mincuzzi, F. De Rossi, F. Di Giacomo, A. Reale, A. Di Carlo and T. M. Brown, *Appl. Energy*, 2014, **113**, 1155–1161.
45 H. Arakawa, T. Yamaguchi, T. Sutou, Y. Koishi, N. Tobe, D. Matsumoto and T. Nagai, *Curr. Appl. Phys.*, 2010, **10**, S157–S160.
46 V. Zardetto, F. Di Giacomo, D. Garcia-Alonso, W. Keuning, M. Creatore, C. Mazzuca, A. Reale, A. Di Carlo and T. M. Brown, *Adv. Energy Mater.*, 2013, **3**, 1292–1298.
47 M. Berginc, U. Opara Krašovec, M. Jankovec and M. Topič, *Sol. Energy Mater. Sol. Cells*, 2007, **91**, 821–828.
48 A. Hinsch, J. M. Kroon, R. Kern, I. Uhlendorf, A. Meyer, J. Holzbock and J. Ferber, *Prog. Photovoltaics*, 2001, **9**, 425–438.
49 P. M. Sommeling, M. Späth, H. J. P. Smit, N. J. Bakker and J. M. Kroon, *J. Photochem. Photobiol., A*, 2004, **164**, 137–144.
50 E. Skoplaki and J. A. Palyvos, *Sol. Energy*, 2009, **83**, 614–624.
51 K. L. Ray, Bachelor of Science Thesis, Massachusetts Institute of Technology, 2010.
52 J. Kalowekamo and E. Baker, *Sol. Energy*, 2009, **83**, 1224–1231.
53 N. Tanabe, *Fujikura Tech. Rev.*, 2010.
54 D. M. Powell, M. T. Winkler, H. J. Choi, C. B. Simmons, D. B. Needleman and T. Buonassisi, *Energy Environ. Sci.*, 2012, **5**, 5874–5883.
55 Z. M. Beiley and M. D. McGehee, *Energy Environ. Sci.*, 2012, **5**, 9173–9179.
56 B. Azzopardi, C. J. M. Emmott, A. Urbina, F. C. Krebs, J. Mutale and J. Nelson, *Energy Environ. Sci.*, 2011, **4**, 3741–3753.
57 G. Hashmi, K. Miettunen, T. Peltola, J. Halme, I. Asghar, K. Aitola, M. Toivola and P. Lund, *Renewable Sustainable Energy Rev.*, 2011, **15**, 3717–3732.
58 A. H. Ip, S. M. Thon, S. Hoogland, O. Voznyy, D. Zhitomirsky, R. Debnath, L. Levina, L. R. Rollny, G. H. Carey, A. Fischer, K. W. Kemp, I. J. Kramer, Z. Ning,

A. J. Labelle, K. W. Chou, A. Amassian and E. H. Sargent, *Nat. Nanotechnol.*, 2012, **7**, 577–582.
59 T. Meyer, M. S. Asef Azam, D. Martineau, F. Oswald, S. Narbey, G. Laporte, R. Cisneros, G. Tregnano and A. Meyer, *CleanTechDay 3rd Generation Photovoltaics*, CSEM, Basel, 2009.
60 A. Kay and M. Grätzel, *Sol. Energy Mater. Sol. Cells*, 1996, **44**, 99–117.
61 H. Pettersson, K. Nonomura, L. Kloo and A. Hagfeldt, *Energy Environ. Sci.*, 2012, **5**, 7376–7380.
62 D. K. Benson and H. M. Branz, *Sol. Energy Mater. Sol. Cells*, 1995, **39**, 203–211.
63 H. Zhou, T. B. Song, C. H. Chung, B. Lei, B. Bob, R. Zhu, H. S. Duan, C. J. Hsu and Y. Yang, *Adv. Energy Mater.*, 2012, **2**, 1368–1374.
64 C. López-López, S. Colodrero, M. E. Calvo and H. Míguez, *Energy Environ. Sci.*, 2013, **6**, 1260–1266.
65 Z. Xie, X. Jin, G. Chen, J. Xu, D. Chen and G. Shen, *Chem. Commun.*, 2014, **50**, 608–610.
66 K. Wang, H. Wu, Y. Meng, Y. Zhang and Z. Wei, *Energy Environ. Sci.*, 2012, **5**, 8384–8389.
67 D. Wei, M. R. J. Scherer, C. Bower, P. Andrew, T. Ryhänen and U. Steiner, *Nano Lett.*, 2012, **12**, 1857–1862.
68 V. K. Thakur, G. Ding, J. Ma, P. S. Lee and X. Lu, *Adv. Mater.*, 2012, **24**, 4071–4096.
69 S. Yang, J. Zheng, M. Li and C. Xu, *Sol. Energy Mater. Sol. Cells*, 2012, **97**, 186–190.
70 P. K. Shen, H. T. Huang and A. C. C. Tseung, *J. Electrochem. Soc.*, 1992, **139**, 1840–1845.
71 Q. Zhong, J. R. Dahn and K. Colbow, *Phys. Rev. B: Condens. Matter Mater. Phys.*, 1992, **46**, 2554–2560.
72 J. P. Cronin, D. J. Tarico, J. C. L. Tonazzi, A. Agrawal and S. R. Kennedy, *Sol. Energy Mater. Sol. Cells*, 1993, **29**, 371–386.
73 M. Deepa, M. Kar and S. A. Agnihotry, *Thin Solid Films*, 2004, **468**, 32–42.
74 V. Kumar, N. Singh, V. Kumar, L. P. Purohit, A. Kapoor, O. M. Ntwaeaborwa and H. C. Swart, *J. Appl. Phys.*, 2013, **114**, 134506.
75 R. Baetens, B. P. Jelle and A. Gustavsen, *Sol. Energy Mater. Sol. Cells*, 2010, **94**, 87–105.
76 C. Bechinger, S. Ferrere, A. Zaban, J. Sprague and B. A. Gregg, *Nature*, 1996, **383**, 608–610.
77 C. Bechinger and B. A. Gregg, *Sol. Energy Mater. Sol. Cells*, 1998, **54**, 405–410.
78 L.-M. Huang, C.-W. Hu, H.-C. Liu, C.-Y. Hsu, C.-H. Chen and K.-C. Ho, *Sol. Energy Mater. Sol. Cells*, 2012, **99**, 154–159.
79 K.-S. Ahn, S. J. Yoo, M.-S. Kang, J.-W. Lee and Y.-E. Sung, *J. Power Sources*, 2007, **168**, 533–536.
80 J. Maçaira, L. Andrade and A. Mendes, *Renewable Sustainable Energy Rev.*, 2013, **27**, 334–349.
81 D. D'Ercole, L. Dominici, T. M. Brown, F. Michelotti, A. Reale and A. Di Carlo, *Appl. Phys. Lett.*, 2011, **99**, 213301.
82 Solaronix NEWS, http://www.solaronix.com/news/ccrdelivery/, accessed January 2014.
83 Dyesol NEWS, http://www.dyesol.com/partners/current-projects, accessed December 2013.
84 L. Han, A. Fukui, Y. Chiba, A. Islam, R. Komiya, N. Fuke, N. Koide, R. Yamanaka and M. Shimizu, *Appl. Phys. Lett.*, 2009, **94**, 013305.
85 E. J. W. Crossland, N. Noel, V. Sivaram, T. Leijtens, J. A. Alexander-Webber and H. J. Snaith, *Nature*, 2013, **495**, 215–219.
86 A. S. Hey and H. J. Snaith, *J. Appl. Phys.*, 2013, **114**, 183105.
87 F. Matteocci, S. Casaluci, S. Razza, A. Guidobaldi, T. M. Brown, A. Reale and A. Di Carlo, *J. Power Sources*, 2014, **246**, 361–364.
88 S. A. Agarkar, V. V. Dhas, S. Muduli and S. B. Ogale, *RSC Adv.*, 2012, **2**, 11645–11649.
89 J. G. Kang, J. H. Kim and J. T. Kim, *Int. J. Photoenergy*, 2013, 472086.
90 Dyesol Media, http://www.dyesol.com/posts/cat/corporate-news/post/dyesol-achieves-technical-breakthrough/, accessed December 2013.
91 N. Jiang, T. Sumitomo, T. Lee, A. Pellaroque, O. Bellon, D. Milliken and H. Desilvestro, *Sol. Energy Mater. Sol. Cells*, 2013, **119**, 36–50.
92 H. Pettersson, T. Gruszecki, R. Bernhard, L. Häggman, M. Gorlov, G. Boschloo, T. Edvinsson, L. Kloo and A. Hagfeldt, *Prog. Photovoltaics*, 2007, **15**, 113–121.
93 S. Ito, T. N. Murakami, P. Comte, P. Liska, C. Grätzel, M. K. Nazeeruddin and M. Grätzel, *Thin Solid Films*, 2008, **516**, 4613–4619.
94 M. Späth, P. M. Sommeling, J. A. M. Van Roosmalen, H. J. P. Smit, N. P. G. Van Der Burg, D. R. Mahieu, N. J. Bakker and J. M. Kroon, *Prog. Photovoltaics*, 2003, **11**, 207–220.
95 R. Sastrawan, J. Beier, U. Belledin, S. Hemming, A. Hinsch, R. Kern, C. Vetter, F. M. Petrat, A. Prodi-Schwab, P. Lechner and W. Hoffmann, *Sol. Energy Mater. Sol. Cells*, 2006, **90**, 1680–1691.
96 S. Dai, J. Weng, Y. Sui, C. Shi, Y. Huang, S. Chen, X. Pan, X. Fang, L. Hu, F. Kong and K. Wang, *Sol. Energy Mater. Sol. Cells*, 2004, **84**, 125–133.
97 W. J. Lee, E. Ramasamy, D. Y. Lee and J. S. Song, *Sol. Energy Mater. Sol. Cells*, 2007, **91**, 1676–1680.
98 F. Giordano, E. Petrolati, T. M. Brown, A. Reale and A. Di Carlo, *IEEE Trans. Electron Devices*, 2011, **58**, 2759–2764.
99 S. Mastroianni, A. Lanuti, S. Penna, A. Reale, T. M. Brown, A. Di Carlo and F. Decker, *ChemPhysChem*, 2012, **13**, 2925–2936.
100 A. Hinsch, H. Brandt, W. Veurman, S. Hemming, M. Nittel, U. Würfel, P. Putyra, C. Lang-Koetz, M. Stabe, S. Beucker and K. Fichter, *Sol. Energy Mater. Sol. Cells*, 2009, **93**, 820–824.
101 M. Ikegami, J. Suzuki, K. Teshima, M. Kawaraya and T. Miyasaka, *Sol. Energy Mater. Sol. Cells*, 2009, **93**, 836–839.
102 F. Giordano, A. Guidobaldi, E. Petrolati, L. Vesce, R. Riccitelli, A. Reale, T. M. Brown and A. Di Carlo, *Prog. Photovoltaics*, 2013, **21**, 1653–1658.

103 N. Kato, Y. Takeda, K. Higuchi, A. Takeichi, E. Sudo, H. Tanaka, T. Motohiro, T. Sano and T. Toyoda, *Sol. Energy Mater. Sol. Cells*, 2009, **93**, 893–897.

104 L. Wang, X. Fang and Z. Zhang, *Renewable Sustainable Energy Rev.*, 2010, **14**, 3178–3184.

105 J. M. Kroon, Energy Research Center report, 2005, ECN-C-05-078, 1–41.

106 Y. Takeda, N. Kato, K. Higuchi, A. Takeichi, T. Motohiro, S. Fukumoto, T. Sano and T. Toyoda, *Sol. Energy Mater. Sol. Cells*, 2009, **93**, 808–811.

107 Y. Jun, J.-H. Son, D. Sohn and M. G. Kang, *J. Photochem. Photobiol., A*, 2008, **200**, 314–317.

108 T. S. Toyodaa, J. Nakajimaa, S. Doia, S. Fukumotoa, A. Itoa, T. Tohyamaa, M. Yoshidaa, T. Kanagawaa, T. Motohirob, T. Shigab, K. Higuchib, H. Tanakab, H. Takedab, T. Fukanob, N. Katohb, A. Takeichib, K. Takechib and M. Shiozawab, *Photochem. Photobiol.*, 2004, **164**, 203–207.

109 J. A. Hopkins, G. Phani and I. L. Skryabin, Google Patents, 2006.

110 S. Dai, J. Weng, Y. Sui, C. Shi, Y. Huang, S. Chen, X. Pan, X. Fang, L. Hu, F. Kong and K. Wang, *Sol. Energy Mater. Sol. Cells*, 2004, **84**, 125–133.

111 K. Okada, H. Matsui, T. Kawashima, T. Ezure and N. Tanabe, *J. Photochem. Photobiol., A*, 2004, **164**, 193–198.

112 J. M. Kroon, N. J. Bakker, H. J. P. Smit, P. Liska, K. R. Thampi, P. Wang, S. M. Zakeeruddin, M. Grätzel, A. Hinsch, S. Hore, U. Würfel, R. Sastrawan, J. R. Durrant, E. Palomares, H. Pettersson, T. Gruszecki, J. Walter, K. Skupien and G. E. Tulloch, *Prog. Photovoltaics*, 2007, **15**, 1–18.

113 S. Dai, J. Weng, Y. Sui, S. Chen, S. Xiao, Y. Huang, F. Kong, X. Pan, L. Hu, C. Zhang and K. Wang, *Inorg. Chim. Acta*, 2008, **361**, 786–791.

114 T. C. Wei, J. L. Lan, C. C. Wan, W. C. Hsu and Y. H. Chang, *Prog. Photovoltaics*, 2012, **21**, 1625–1633.

115 G. R. A. Kumara, S. Kawasaki, P. V. V. Jayaweera, E. V. A. Premalal and S. Kaneko, *Thin Solid Films*, 2012, **520**, 4119–4121.

116 J. Takashima, T. Fujii and K. Furusaki, *Electrochem. Soc. meeting*, 2008, **MA2008-02**, 478.

117 Y. D. Zhang, X. M. Huang, K. Y. Gao, Y. Y. Yang, Y. H. Luo, D. M. Li and Q. B. Meng, *Sol. Energy Mater. Sol. Cells*, 2011, **95**, 2564–2569.

118 F. Pichot, J. R. Pitts and B. A. Gregg, *Langmuir*, 2000, **16**, 5626–5630.

119 T. Kado, M. Yamaguchi, Y. Yamada and S. Hayase, *Chem. Lett.*, 2003, **32**, 1056–1057.

120 K. Fan, T. Peng, J. Chen, X. Zhang and R. Li, *J. Mater. Chem.*, 2012, **22**, 16121–16126.

121 K. Fan, R. Li, J. Chen, W. Shi and T. Peng, *Sci. Adv. Mater.*, 2013, **5**, 1596–1626.

122 Solaronix Webshop, http://shop.solaronix.com/electrode-materials.html, accessed May 2014.

123 H.-P. Jen, M.-H. Lin, L.-L. Li, H.-P. Wu, W.-K. Huang, P.-J. Cheng and E. W.-G. Diau, *ACS Appl. Mater. Interfaces*, 2013, **5**, 10098–10104.

124 Y. Jun, J. Kim and M. G. Kang, *Sol. Energy Mater. Sol. Cells*, 2007, **91**, 779–784.

125 L. Yang, U. B. Cappel, E. L. Unger, M. Karlsson, K. M. Karlsson, E. Gabrielsson, L. Sun, G. Boschloo, A. Hagfeldt and E. M. J. Johansson, *Phys. Chem. Chem. Phys.*, 2012, **14**, 779–789.

126 H. C. Weerasinghe, F. Huang and Y.-B. Cheng, *Nano Energy*, 2013, **2**, 174–189.

127 J. M. Macák, H. Tsuchiya and P. Schmuki, *Angew. Chem., Int. Ed.*, 2005, **44**, 2100–2102.

128 C. A. Grimes, *J. Mater. Chem.*, 2007, **17**, 1451–1457.

129 D. Kuang, J. Brillet, P. Chen, M. Takata, S. Uchida, H. Miura, K. Sumioka, S. M. Zakeeruddin and M. Grätzel, *ACS Nano*, 2008, **2**, 1113–1116.

130 M. Dürr, A. Schmid, M. Obermaier, S. Rosselli, A. Yasuda and G. Nelles, *Nat. Mater.*, 2005, **4**, 607–611.

131 G. Boschloo, H. Lindström, E. Magnusson, A. Holmberg and A. Hagfeldt, *J. Photochem. Photobiol., A*, 2002, **148**, 11–15.

132 M. Dürr, A. Yasuda and G. Nelles, *Appl. Phys. Lett.*, 2006, **89**, 061110.

133 L. Yang, L. Wu, M. Wu, G. Xin, H. Lin and T. Ma, *Electrochem. Commun.*, 2010, **12**, 1000–1003.

134 H. W. Chen, C. Y. Lin, Y. H. Lai, J. G. Chen, C. C. Wang, C. W. Hu, C. Y. Hsu, R. Vittal and K. C. Ho, *J. Power Sources*, 2011, **196**, 4859–4864.

135 S. Senthilarasu, T. A. N. Peiris, J. García-Cañadas and K. G. U. Wijayantha, *J. Phys. Chem. C*, 2012, **116**, 19053–19061.

136 D. Zhang, T. Yoshida, T. Oekermann, K. Furuta and H. Minoura, *Adv. Funct. Mater.*, 2006, **16**, 1228–1234.

137 L. Vesce, R. Riccitelli, G. Soscia, T. M. Brown, A. Di Carlo and A. Reale, *J. Non-Cryst. Solids*, 2010, **356**, 1958–1961.

138 S. W. Lee, *Mol. Cryst. Liq. Cryst.*, 2011, **551**, 172–180.

139 S. I. Noh, K. N. Bae, H. J. Ahn and T. Y. Seong, *Ceram. Int.*, 2013, **39**, 8097–8101.

140 J. Wu, Y. Xiao, Q. Tang, G. Yue, J. Lin, M. Huang, Y. Huang, L. Fan, Z. Lan, S. Yin and T. Sato, *Adv. Mater.*, 2012, **24**, 1884–1888.

141 M. Biancardo, K. West and F. C. Krebs, *Sol. Energy Mater. Sol. Cells*, 2006, **90**, 2575–2588.

142 J. Nei de Freitas, C. Longo, A. F. Nogueira and M.-A. De Paoli, *Sol. Energy Mater. Sol. Cells*, 2008, **92**, 1110–1114.

143 A. Hinsch, W. Veurman, H. Brandt, R. Loayza Aguirre, K. Bialecka and K. Flarup Jensen, *Prog. Photovoltaics*, 2012, **20**, 698–710.

144 Y. Liu, H. Wang, H. Shen and W. Chen, *Appl. Energy*, 2010, **87**, 436–441.

145 T. C. Wei, S. P. Feng, Y. H. Chang, S. J. Cherng, Y. J. Lin, C. M. Chen and H. H. Chen, *Int. J. Electrochem. Sci.*, 2012, **7**, 11904–11916.

146 R. Sastrawan, J. Renz, C. Prahl, J. Beier, A. Hinsch and R. Kern, *J. Photochem. Photobiol., A*, 2006, **178**, 33–40.

147 C. Cornaro, S. Bartocci, D. Musella, C. Strati, A. Lanuti, S. Mastroianni, S. Penna, A. Guidobaldi, F. Giordano, E. Petrolati, T. M. Brown, A. Reale and A. Di Carlo, *Prog. Photovoltaics*, 2013, **21**, 1–11.

148 A. Yella, H.-W. Lee, H. N. Tsao, C. Yi, A. K. Chandiran, M. K. Nazeeruddin, E. W.-G. Diau, C.-Y. Yeh, S. M. Zakeeruddin and M. Grätzel, *Science*, 2011, **334**, 629–634.

149 Y. Chiba, A. Islam, Y. Watanabe, R. Komiya, N. Koide and L. Han, *Jpn. J. Appl. Phys.*, 2006, **45**, L638–L640.

150 S. Schiefer, B. Zimmermann and U. Würfel, *Sol. Energy Mater. Sol. Cells*, 2013, **115**, 29–35.

151 I. Chung, B. Lee, J. He, R. P. H. Chang and M. G. Kanatzidis, *Nature*, 2012, **485**, 486–489.

152 T. C. Wei, J. L. Lan, C. C. Wan, W. C. Hsu and Y. H. Chang, *Prog. Photovoltaics*, 2013, **21**, 1625–1633.

153 A. Fakharuddin, P. S. Archana, Z. Kalidin, M. M. Yusoff and R. Jose, *RSC Adv.*, 2013, **3**, 2683–2689.

154 R. Jose, A. Fakharuddin, P. S. Archana and M. M. Yusoff, *Ab. Am. Chem. Soc.*, American Chemical Society spring meeting, New Orleans USA, 2013, vol. 245.

155 A. Fakharuddin, I. Ahmed, Z. Khalidin, M. M. Yusoff and R. Jose, *Appl. Phys. Lett.*, 2014, **104**, 053905.

156 A. Fakharuddin, I. Ahmed, Z. Khalidin, M. M. Yusoff and R. Jose, *J. Appl. Phys.*, 2014, **115**, 164509.

157 A. Fakharuddin, I. Ahmed, Q. Wali, Z. Khalidin, M. M. Yusoff and R. Jose, *Adv. Mater. Res.*, 2014, **295**, 553–558.

158 J. Nelson, *Phys. Rev. B: Condens. Matter Mater. Phys.*, 1999, **59**, 15374–15380.

159 J. Bisquert, *J. Phys. Chem. C*, 2007, **111**, 17163–17168.

160 J. P. Gonzalez-Vazquez, J. A. Anta and J. Bisquert, *Phys. Chem. Chem. Phys.*, 2009, **11**, 10359–10367.

161 A. B. F. Martinson, M. r. S. Góes, F. Fabregat-Santiago, J. Bisquert, M. J. Pellin and J. T. Hupp, *J. Phys. Chem. A*, 2009, **113**, 4015–4021.

162 A. Gagliardi, D. Gentilini and A. D. Carlo, *J. Phys. Chem. C*, 2012, **116**, 23882–23889.

163 G. J. Nelson, B. N. Cassenti, A. A. Peracchio and W. K. S. Chiu, *Electrochim. Acta*, 2013, **90**, 475–481.

164 J. R. Jennings and L. M. Peter, *J. Phys. Chem. C*, 2007, **111**, 16100–16104.

165 J. P. Gonzalez-Vazquez, J. A. Anta and J. Bisquert, *J. Phys. Chem. C*, 2010, **114**, 8552–8558.

166 J. Navas, E. Guillén, R. Alcántara, C. Fernaández-Lorenzo, J. Martín-Calleja, G. Oskam, J. Idígoras, T. Berger and J. A. Anta, *J. Phys. Chem. Lett.*, 2011, **2**, 1045–1050.

167 F. Fabregat-Santiago, J. Bisquert, E. Palomares, L. Otero, D. Kuang, S. M. Zakeeruddin and M. Grätzel, *J. Phys. Chem. C*, 2007, **111**, 6550–6560.

168 P. M. K. Sommeling and J. M. Kroon, *24th European Photovoltaic Solar Energy Conference and Exhibition*, Hamburg, Germany, 2009.

169 M. I. Asghar, K. Miettunen, J. Halme, P. Vahermaa, M. Toivola, K. Aitola and P. Lund, *Energy Environ. Sci.*, 2010, **3**, 418–426.

170 R. Kern, V. D. Burg, G. Chmiel, J. Ferber, G. Hasenhindl, A. Hinsch, R. Kinderman, J. M. Kroon, A. Meyer, T. Meyer, R. Niepmann, J. A. M. van Roosmalen, C. Schill, P. Sommeling, M. Späth and I. Uhlendorf, *Opto-Electron. Rev.*, 2000, **8**, 284–288.

171 J. M. Kroon, A. Hinsch, J. A. M. van Roosmalen, N. P. G. van der Burg, N. J. Bakker, R. Kinderman, P. M. Sommeling, M. Späth, R. Kern, R. Sastrawan, J. Ferber, M. Schubert, G. Hasenhindl, C. Schill, M. Lorenz, R. Stangl, S. Baumgärtner, C. Peter, A. Meyer, T. Meyer, I. Uhlendorf, J. Holzbock and R. Niepmann, *Energy Research Center report*, 2001, JOR3-CT98-0261, 1–11.

172 P. Wang, C. Klein, R. Humphry-Baker, S. M. Zakeeruddin and M. Grätzel, *Appl. Phys. Lett.*, 2005, **86**, 123508.

173 P. Wang, S. M. Zakeeruddin, J.-E. Moser, M. K. Nazeeruddin, T. Sekiguchi and M. Grätzel, *Nat. Mater.*, 2003, **2**, 402.

174 P. Wang, S. M. Zakeeruddin, R. Humphry-Baker, J.-E. Moser and M. Grätzel, *Adv. Mater.*, 2003, **15**, 2101.

175 B. Macht, M. Turrión, A. Barkschat, P. Salvador, K. Ellmer and H. Tributsch, *Sol. Energy Mater. Sol. Cells*, 2002, **73**, 163–173.

176 S. Mastroianni, I. Asghar, K. Miettunen, J. Halme, A. Lanuti, T. M. Brown and P. Lund, *Phys. Chem. Chem. Phys.*, 2014, **16**, 6092–6100.

177 H. B. K. F. Jensen, C. Im, J. Wilde and A. Hinsch, *presented in part at the 28th European PV Solar Energy Conference and Exhibition*, Paris, France, 2013.

178 A. G. Kontos, T. Stergiopoulos, V. Likodimos, D. Milliken, H. Desilvesto, G. Tulloch and P. Falaras, *J. Phys. Chem. C*, 2013, **117**, 8636–8646.

179 J. M. Kroon, P. M. Sommeling, N. J. Bakker, H. van Mansom, A. Hinsch, W. Veurman, H. Pettersson, T. Gruszecki, B. C. O'Regan, F. Sauvage, S. M. Zakeeruddin, M. Grätzel, E. Palomares, J. Clifford, E. Martínez, T. Torres, M. Feigenson, B. Breen, S. Vallon, S. Logunov and M. Spratt, *25th European Photovoltaic Solar Energy Conference and Exhibition*, Valencia, Spain, 2010, pp. 306–311.

180 K.-M. Lee, C.-Y. Chen, Y.-T. Tsai, L.-C. Lin and C.-G. Wu, *RSC Adv.*, 2013, **3**, 9994–10000.

181 J. Goldstein, I. Yakupov and B. Breen, *Sol. Energy Mater. Sol. Cells*, 2010, **94**, 638–641.

182 X. Wang, R. Deng, S. A. Kulkarni, X. Wang, S. S. Pramana, C. C. Wong, M. Gratzel, S. Uchida and S. G. Mhaisalkar, *J. Mater. Chem. A*, 2013, **1**, 4345–4351.

183 S. Mastroianni, A. Lembo, T. M. Brown, A. Reale and A. Di Carlo, *ChemPhysChem*, 2012, **13**, 2964–2975.

184 S. Mastroianni, A. Lanuti, T. M. Brown, R. Argazzi, S. Caramori, A. Reale and A. Di Carlo, *Appl. Phys. Lett.*, 2012, **101**, 123302.

185 T. Y. Hirnori Arakawa, K. Okada, H. Masturi, T. Kitamura, N. Tanabe, *Vol. Fujikura Technical Reviews*, 2009, pp. 55–60.

186 C. B. Claudia Barolo, R. Boaretto, T. Brown, L. Bonandini, E. Busatto, S. Caramori, D. Colonna, G. De Angelis, A. Di Carlo, A. Guglielmotti, A. L. Andrea Guidobaldi, A. Lembo, D. Magistri, V. Mirruzzo, S. Penna, S. Pietrantoni, D. Prencipe, A. Reale, R. Riccitelli, A. Smarra, G. Soscia, R. Tagliaferro, L. Vesce, G. Viscardi and P. Mariani, proceeding of HOPV14, page 72, 2014.

187 X. Yang, M. Yanagida and L. Han, *Energy Environ. Sci.*, 2013, **6**, 54–66.

188 L. Tillemann, http://energy.gov/sites/prod/files/2013/09/f2/200130917-revolution-now.pdf, *U.S. Department of Energy*, 2013.
189 H. Zervos, http://www.idtechex.com/research/reports/dye-sensitized-solar-cellsdssc-dsc-2013-2023-technologies-markets-players-000345.asp?viewopt%BCshowall&viewopt=contents, ID-TechEx, 2013.
190 S. Yoon, S. Tak, J. Kim, Y. Jun, K. Kang and J. Park, *Build. Environ.*, 2011, **46**, 1899–1904.
191 A. Reale, L. Cinà, A. Malatesta, R. De Marco, T. M. Brown and A. Di Carlo, *Energ. Tech.*, 2014, **2**, 531–541.